Extratropical Air-Sea Interaction, Sea Surface Temperature Variability, and the Pacific Decadal Oscillation

Michael Alexander

Earth System Research Laboratory, NOAA, Boulder, Colorado, USA

We examine processes that influence North Pacific sea surface temperature (SST) anomalies including surface heat fluxes, upper ocean mixing, thermocline variability, ocean currents, and tropical-extratropical interactions via the atmosphere and ocean. The ocean integrates rapidly varying atmospheric heat flux and wind forcing, and thus a stochastic model of the climate system, where white noise forcing produces a red spectrum, appears to provide a baseline for SST variability even on decadal time scales. However, additional processes influence Pacific climate variability including the "reemergence mechanism," where seasonal variability in mixed layer depth allows surface temperature anomalies to be stored at depth during summer and return to the surface in the following winter. Wind stress curl anomalies in the central/east Pacific drive thermocline variability that propagates to the west Pacific via baroclinic Rossby waves and influences SST by vertical mixing and the change in strength and position of the ocean gyres. Atmospheric changes associated with the El Niño–Southern Oscillation (ENSO) also influence North Pacific SST anomalies via the "atmospheric bridge." The dominant pattern of North Pacific SST anomalies, the Pacific Decadal Oscillation (PDO), exhibits variability on interannual as well as decadal time scales. Unlike ENSO, the PDO does not appear to be a mode of the climate system, but rather it results from several different mechanisms including (1) stochastic heat flux forcing associated with random fluctuations in the Aleutian Low, (2) the atmospheric bridge augmented by the reemergence mechanism, and (3) wind-driven changes in the North Pacific gyres.

1. INTRODUCTION

There are several reasons why the oceans play a key role in climate variability at interannual and longer time scales. Because of the high specific heat and density of seawater, the heat capacity of an ocean column ~2.5 m deep is as large as the entire atmosphere above it. In addition, the upper ocean is generally well mixed, and sea surface temperature anomalies (SSTAs) extend over the depth of the mixed layer tens to hundreds of meters below the surface. As a result, SSTA, the primary means through which the ocean influences the atmosphere, can persist for months or even years. In addition to thermodynamic considerations, many dynamical ocean processes are much slower than their atmospheric counterparts. For example, relatively strong currents such as the Gulf Stream and Kuroshio are on the order of 1 m s^{-1}, roughly 2 orders of magnitude slower than the jet stream in similar locations. Midlatitude ocean gyres take 5–10 years to fully adjust to the wind forcing that drives them, and exchanges with the deeper oceans, via meridional overturning circulations, can take decades to centuries.

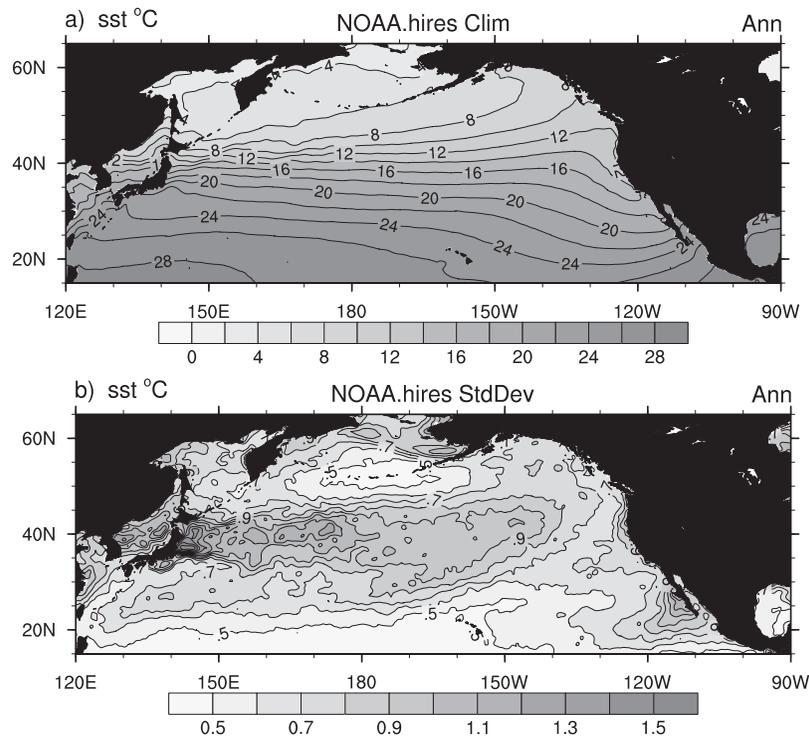Beginning with the pioneering work of *Namias* [e.g., 1959, 1963, 1965, 1969] and *Bjerknes* [1964], many studies

Figure 1. (a) Annual mean and (b) standard deviation of SST for the years 1985–2007 obtained from the NOAA high-resolution (0.25° latitude × longitude) SST data set [*Reynolds et al.*, 2007].

have sought to understand the temporal and spatial structure of midlatitude SSTAs and the extent to which they influence the atmosphere. The dominant pattern of sea surface temperature (SST) variability over the North Pacific exhibited pronounced low-frequency fluctuations during the 20th century and was thus termed the Pacific Decadal Oscillation (PDO) by *Mantua et al.* [1997]. The fluctuations in the PDO have been linked to many climatic and ecosystem changes
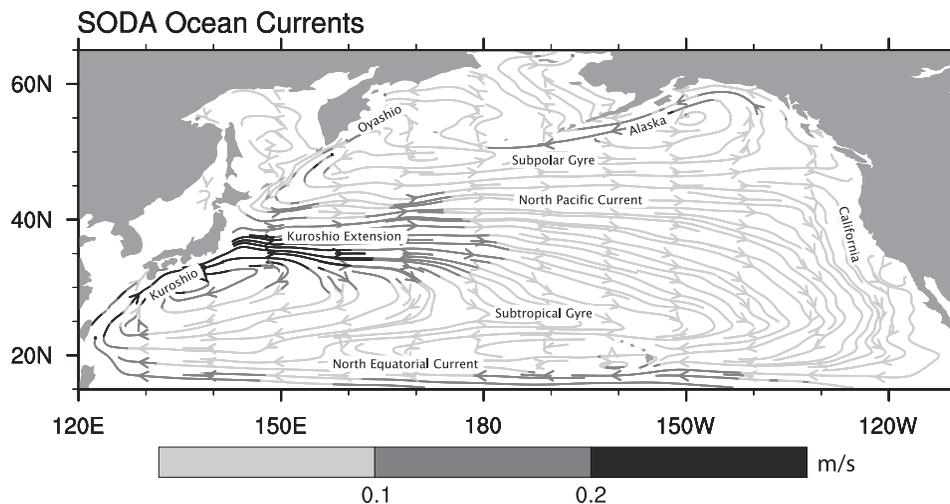

Figure 2. Annual average ocean currents (m s^{-1}) averaged over the upper 500 m from the Simple Ocean Data Assimilation (SODA) [*Carton and Giese*, 2008] for the years 1958–2001. The current strength is indicated by the three-tone gray scale with maximum values of ~0.7 m s^{-1} in the Kuroshio Current.

and thus have become a focal point for studies of Pacific climate variability. In this chapter, we examine processes that influence extratropical SST anomalies and mechanisms for generating Pacific decadal variability including the PDO.

This chapter is structured as follows: basic properties of the North Pacific Ocean including the mean SST and its interannual variability, the vertical structure of temperature, and the three-dimensional flow are described in section 2; the terms that contribute to the surface heat budget and thus the SST tendency are examined in section 3; the processes that generate and maintain North Pacific SST anomalies, including stochastic forcing, upper ocean mixing, ocean currents and Rossby waves, dynamic extratropical air-sea interaction, and teleconnections from the tropics are explored in section 4. The PDO and its underlying causes are described in section 5, while section 6 examines other potential sources of Noth Pacific variability and processes/ patterns that occur in other extratropical ocean basins.
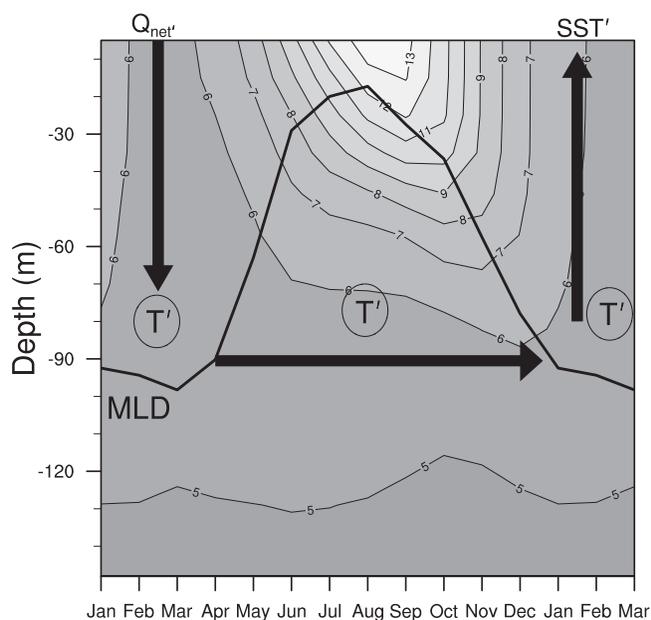

Figure 3. Mean ocean temperature (°C) and mixed layer depth (h) over the course of the seasonal cycle in a $5° \times 5°$ box centered on 50°N, 145°W (where weather ship P was located from the 1950s to the 1980s) in the northeast Pacific. The temperature values are from SODA, and the h values are from *Monterey and Levitus* [1997]. Arrows denote the reemergence mechanism where surface heat flux anomalies create temperature anomalies over the deep winter mixed layer; the anomalies are then sequestered in the summer seasonal thermocline and return to the surface in the following winter.

2. MEAN UPPER OCEAN CLIMATE

North Pacific SST variability is strongly shaped by the climate and circulation of the upper ocean. The mean SST field features nearly zonal isotherms across most of the Pacific with a strong gradient near 40°N, indicative of the subpolar front (consisting of the Oyashio and Kuroshio fronts with a mixed water region in between) that separates the two main gyres in the North Pacific (Figure 1a). In the eastern Pacific, the curvature of the isotherms is consistent with the structure of the currents where the subpolar gyre turns north and the subtropical gyre turns south (Figure 2). The weaker subtropical front, which is more prominent in the SST standard deviation (σ) field (Figure 1b) than in the mean SST field, extends southwestward from approximately 35°N, 135°W to 20°N, 180°. The mean isotherms bulge north in the vicinity of southern Japan associated with the warm water transport by the Kuroshio Current, which turns eastward between 35° and 40°N as the Kuroshio Extension (KE) and then the North Pacific Current. SST variance maxima are located along the KE/subpolar front and the subtropical front, in the Bering Sea, and along the coast of North America (Figure 1b).

The surface layer over most of the world's oceans is vertically well mixed, and thus heating/cooling from the atmosphere spreads from the surface down to the base of the mixed layer (h). Owing to the large thermal inertia of the surface layer, SSTs reach a maximum in August–September and a minimum in March (Figure 3), about 3 months after the respective maximum and minimum in solar forcing, compared to a 1 month lag for land temperatures. Beneath the warm shallow mixed layer in summer lies the seasonal thermocline where the temperature rapidly decreases with depth. The mixed layer is deepest in late winter, when it ranges from 100 m over much of the North Pacific to 200 m in the KE region but shoals to around 20–30 m in late spring and summer (Figures 3 and 4). Since h is approximately 5–20 times smaller in summer than in winter, less energy is required to heat/cool the mixed layer, leading to larger SSTA variability (departures from the seasonal mean) in summer compared with winter.

In the vertical plane, the wind-driven upper ocean circulation consists of a shallow meridional overturning circulation, the subtropical cell (STC) (Figure 5a). In the subtropics and midlatitudes, water subducts; that is, it leaves the mixed layer via downward Ekman pumping and lateral induction via horizontal advection across the sloping base of the mixed layer and enters the main thermocline (Figure 5b). It flows downward and equatorward along isopycnal surfaces where some of the water (1) returns to midlatitudes via the southern and western branches of the
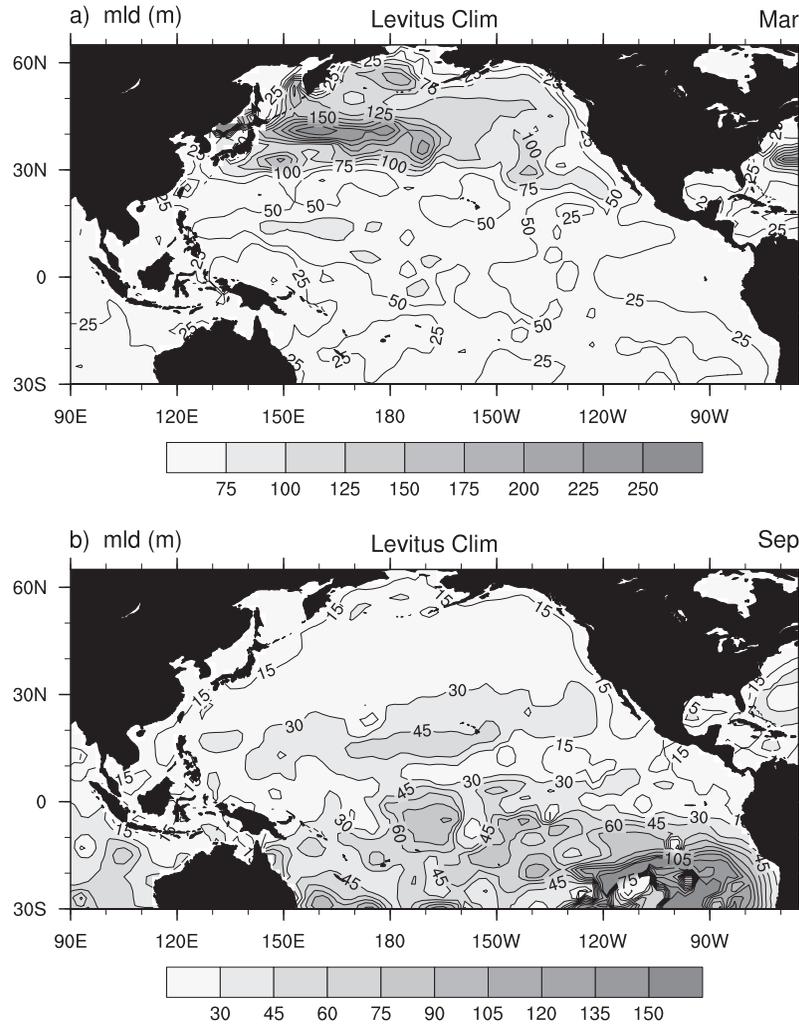
Figure 4. Long-term mean mixed layer depth (m) during (a) March and (b) September using a density difference between the surface and base of the mixed layer of 0.125 kg m^{-3}. Data are from *Monterey and Levitus* [1997].

subtropical gyre, (2) reaches the western boundary equatorward of ~20°S and then flows toward the tropics and then eastward along the equator, or (3) has a convoluted equatorward pathway in the ocean interior (Figure 5b). Water in scenarios 1 and 3 upwells at the equator and then returns to the subtropics in the thin surface Ekman layer (Figure 5a). Observations [*Huang and Qiu*, 1994; *Johnson and McPhaden*, 2001], modeling studies [*McCreary and Lu*, 1994; *Liu*, 1994; *Qu et al.*, 2002], and analyses of transient tracers such as tritium from nuclear bomb tests [*Fine et al.*, 1981, 1983] suggest that subduction zones in the North Pacific contribute much of the water within the equatorial undercurrent, which then reaches the surface in the eastern equatorial Pacific. Thus, variations in the temperature or strength of this cell could alter conditions in the equatorial

Pacific on decadal time scales including modulating ENSO variability.

3. SST TENDENCY SURFACE HEAT BUDGET

Following *Frankignoul* [1985], the SST tendency equation, derived by integrating the heat budget over the mixed layer (ML), can be written as

$$\frac{\partial T_m}{\partial t} = \frac{Q_{net}}{\rho_0 c_p h} + \left(\frac{w + w_e}{h}\right)(T_b - T_m) - \mathbf{v}\cdot\nabla T_m - \frac{Q_{swh}}{\rho_o c_p h} + A\nabla^2 T_m,$$

$$\qquad\quad \text{I} \qquad\qquad\qquad \text{II} \qquad\quad \text{III} \qquad \text{IV} \qquad\quad \text{V} \qquad (1)$$

where T_m is the ML temperature, which is equivalent to the SST for a well-mixed surface layer; Q_{net} is the net surface
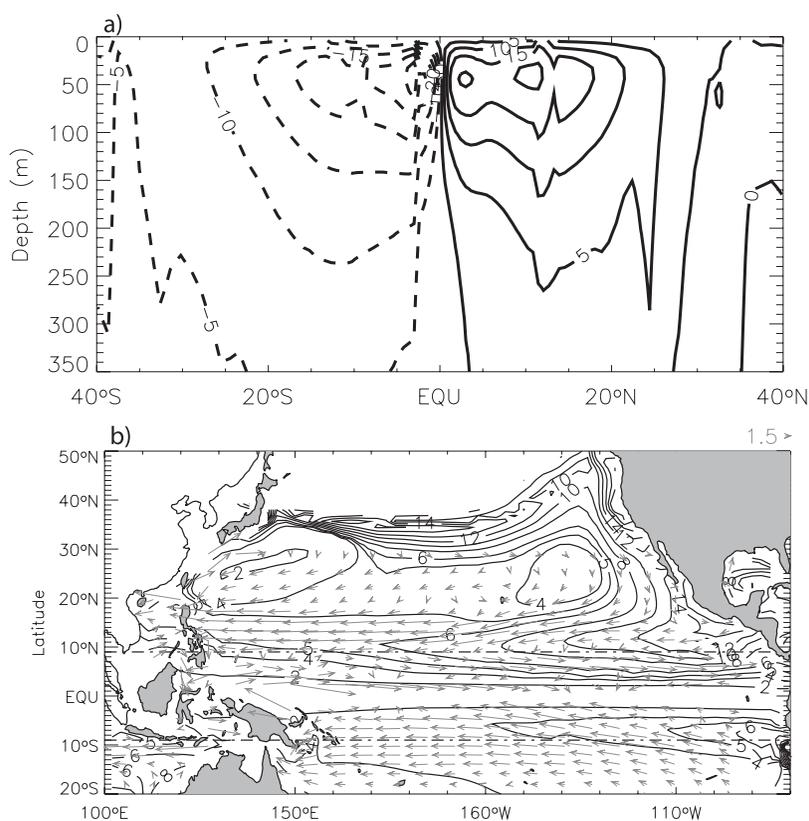
Figure 5. Pacific subtropical cell (STC). (a) Meridional stream function computed from the National Center for Atmospheric Research (NCAR) ocean general circulation model driven by observed atmospheric surface conditions. The flow is clockwise (counterclockwise) in the Northern (Southern) Hemisphere. Contour interval is 5 Sv. (b) Circulation in the subsurface portion of the STC and subtropical gyre. Arrows indicate the averaged upper ocean velocities, integrated from the base of the surface Ekman layer (50 m depth) to the depth of the 25 σ_θ potential density surface; contours denote the mean potential vorticity (PV) on the 25 σ_θ surface, which outcrops between 30°–40°N and the strongest equatorward flow in the subtropics. The currents tend to conserve PV; thus the large values along 10°N act as a partial barrier, and the water subducted in the north Pacific takes a convoluted path to reach the equator. Adapted from *Capotondi et al.* [2005]. © American Meteorological Society. Reprinted with permission.

heat flux; ρ_0 and c_p are the density and specific heat of ocean water, respectively; w is the mean vertical motion; w_e is the entrainment velocity, the turbulent flux through the base of the ML; T_b is the temperature just below the ML; $\mathbf{v}$ is the horizontal velocity, Q_{swh} is the penetrating solar radiation at h; and A is the horizontal diffusion coefficient. The terms in equation (1) are I, surface heating/cooling; II, vertical advection/mixing; III, horizontal advection; IV, sunlight exiting the base of the mixed layer; and V, horizontal diffusion due to eddies.

The net surface heat exchange has four components: the shortwave (Q_{sw}), longwave (Q_{lw}), sensible (Q_{sh}), and latent (Q_{lh}) heat fluxes. Variability in the sensible and latent heat fluxes, which are functions of the near-surface wind speed, air temperature and humidity, and SST, dominate Q_{net} in winter,

since the atmospheric internal variability and mean air-sea temperature difference is much larger during the cold season. Anomalies in Q_{lh} and Q_{sh} are about the same magnitude at high latitudes, while $Q_{lh} \gg Q_{sh}$ in the tropics and subtropics, since warm air holds more moisture and small changes in temperature can lead to large changes in specific humidity (the relative humidity is nearly constant at about 75%–80% over the ocean). Anomalies in Q_{sh} and Q_{lh} are primarily associated with wind speed anomalies in the tropics and subtropics but are more dependent on temperature and humidity anomalies at middle to high latitudes. In general, Q_{lw} varies less than the other three components but is generally in phase with the latent and sensible flux. Fluctuations in cloudiness, especially stratiform clouds, have a strong influence on Q_{sw} over the North Pacific in spring and summer.

In the open ocean, the vertical mass flux into the mixed layer is primarily due to entrainment [*Frankignoul*, 1985; *Alexander*, 1992a], i.e., $w_e > w$, although the latter is critical for driving the ocean circulation. The ML deepens via entrainment; anomalies in w_e are primarily generated by wind stirring in summer and surface cooling in fall and winter [*Alexander et al.*, 2000]. The mixed layer shoals by reforming closer to the surface; there is no entrainment at that time ($w_e = 0$), and h is the depth at which there is a balance between surface heating (positive buoyancy flux), wind stirring, and dissipation. In general, deepening occurs gradually over the cooling season, while the mixed layer shoals fairly abruptly in the spring. Anomalies in h can impact the heat balance of the ML especially in spring and summer: if the ML shoals earlier than usual, the average net heat flux will heat up the thinner surface layer more rapidly, creating positive SST anomalies [*Elsberry and Garwood*, 1978].

Horizontal temperature advection is primarily due to Ekman ($\mathbf{v}_{ek}$) and geostrophic ($\mathbf{v}_g$) currents, although ageostrophic currents associated with eddy activity also impact SST in coastal regions and near western boundary currents. The integrated Ekman transport over the mixed layer is given by $\mathbf{v}_{ek} = -\mathbf{k} \times \tau/\rho_0 f$, where $\mathbf{k}$ is the unit vector, τ is the surface wind stress, and f is the Coriolis parameter; that is, it is $90°$ to the right of the surface wind stress in the Northern Hemisphere. The large-scale currents in the North Pacific are in geostrophic balance and are part of the subtropical and subpolar gyres.

The contribution of the terms in equation (1) to SSTA varies as a function of location, season, and time scale. Q_{net} variability in term I is an important component of the heat budget over most of the Northern Hemisphere oceans from submonthly to decadal time scales and throughout the seasonal cycle. Entrainment impacts SSTA directly via the heat flux through the base of the mixed layer (II) and indirectly through its control of h (in I, II, and IV), which has its greatest impact on SSTA in fall and spring, respectively. Since Ekman currents respond rapidly to changes in the wind, they have nearly an instantaneous impact on SSTA (in III) but can contribute to interannual and longer time scale variability if the wind or SST gradient anomalies are long-lived. Ekman advection contributes to SSTA along the subpolar front and in the central Pacific where strong zonal wind anomalies create anomalous meridional Ekman currents perpendicular to the mean SST gradient. Changes in the large-scale wind fields over the North Pacific generate oceanic Rossby waves that slowly propagate westward. The associated changes in $\mathbf{v}_g$ and the position and strength of the gyres impact SSTs on decadal time scales especially in the KE region. Penetrating solar radiation (IV) and horizontal diffusion (V) are relatively small,

and the latter acts to damp SSTA. For more detailed analyses of the terms contributing to North Pacific SSTA, see *Frankignoul and Reynolds* [1983], *Frankignoul* [1985], *Cayan* [1992a, 1992b, 1992c], *Miller et al.* [1994], *Alexander et al.* [2000], *Qiu* [2000], and *Seager et al.* [2001].

4. PROCESSES THAT GENERATE MIDLATITUDE SSTA (PACIFIC FOCUS)

Equation (1) can be used to interpret theoretical and numerical models of the upper ocean that increase in complexity as more terms on the right-hand side are included. For a motionless ocean with fixed depth h, the temperature (SST) tendency is given by term I; the SST behavior in such a slab ocean can be quite complex given the simplicity of the model. Including term II allows for vertical processes in the ocean, which have been simulated by integral mixed layer models that predict h or layered models that have vertical diffusion between layers. While the Ekman term in III can be represented via heat flux forcing of the mixed layer, the broader impact of currents has been considered from relatively simple shallow water models to full physics regional and general circulation models (GCMs).

4.1. Stochastic Forcing

Hasselmann [1976] proposed that some aspects of climate variability could be represented by a slow system that integrates random or stochastic forcing. Like particles undergoing Brownian motion, the slow climate system exhibits random walk behavior, where the variability increases (decreases) with the square of the period (frequency). *Frankignoul and Hasselmann* [1977] were the first to apply a stochastic model to the real climate system in a study of midlatitude SST variability. The ocean was treated as a motionless slab where the surface heat flux both forces and damps SST anomalies. The forcing represents the passage of atmospheric storms, where the rapid decorrelation time between synoptic events results in a nearly white spectrum (constant as a function of frequency) over the evolution time scale of SST anomalies. The system is damped by a linear negative air-sea feedback, which represents the enhanced (reduced) loss of heat to the atmosphere from anomalously warm (cold) waters and vice versa. The model may be written as

$$\rho ch \frac{dT'_m}{dt} = F' - \lambda T'_m, \qquad (2)$$

where a prime denotes a departure from the time mean, F' is the stochastic atmospheric forcing (constant for white noise), and λ is the linear damping rate whose inverse gives

the decay time. The stochastic model is characterized as a first-order autoregressive, AR1, where the predictable part of T'_m (equivalent to SST) depends only on its value at the previous time. The autocorrelation (r) of an AR1 process decays exponentially, i.e.,

$$r(\tau) = exp[-\lambda\tau/\rho ch], \qquad (3)$$

where τ is the time lag.

The forcing and damping values can be estimated through several different means. If one assumes that the forcing and feedback are entirely through the net heat flux in nature, then F' can be obtained from the Q_{net} variance [*Czaja*, 2003] from simple models of the variables in the bulk formulas [*Frankignoul and Hasselmann*, 1977; *Alexander and Penland*, 1996] or indirectly from the SST variance [*Reynolds*, 1978]. The damping coefficient can be estimated from the SST autocorrelation (e.g., inverting equation (3)), using typical values in the bulk aerodynamic flux

Figure 6. Observed SST variance spectra (black line) in a $5° \times 5°$ box centered on 50°N, 145°W using 134 years of month anomalies from the Hadley Centre HadSST data set [*Rayner et al.*, 2006]. The gray and white curves are based on a AR(1) model, fit to the SST data: $SST_{t+1} = r_{\tau=1}SST_t + \sigma_\varepsilon\varepsilon$, where the noise is given by $\sigma_\varepsilon = [(1 - r^2_{\tau=1})]^2$, σ is the standard deviation and ε is a random number drawn from a Gaussian distribution. The gray shading represents the 5th and 95th percentile bounds for 1200 simulated spectra over 134 years; the white line is the average of simulated spectra and overlays the theoretical spectra on an AR(1) model, the discrete form of equation (4).

formulas [*Lau and Nath*, 1996], the flux response in atmospheric general circulation model (AGCM) experiments to specified SSTAs [*Frankignoul*, 1985], or from the covariance between T_m and Q after removing the ENSO signal [*Frankignoul and Kestenare*, 2002; *Park et al.*, 2005]. Typical λ^{-1} values obtained from these methods are 2–6 months, which corresponds to a flux damping of 10–40 W m^{-2} °C^{-1}, over most of the North Pacific.

The variance spectrum of T'_m from equation (2) may be written as

$$|T'_m(\omega)|^2 = \frac{|F'|^2}{\omega^2 + \lambda^2}, \qquad (4)$$

where ω is the frequency and $|\ |^2$ indicates the variance or power spectrum. At short time scales or high frequencies ($\omega \gg \lambda$), the ocean temperature variance increases with the square of the period (slope of -2 in a log-log spectral plot, Figure 6). At longer time scales ($\omega \ll \lambda$), the damping becomes progressively more important, and the spectrum asymptotes as negative air-sea feedback limits the magnitude of the SST anomalies. This red noise spectrum contains variability on decadal and longer time scales but without spectral peaks. The Hasselmann model has been quite effective at describing the temporal variability of midlatitude SST variability in numerous observational (e.g., Figure 6) and modeling studies and should be considered as the null hypothesis for extratropical SST variability.

Several refinements/extensions have been proposed to the stochastic model for midlatitude SSTs:

1. Additional processes, such as the rapidly varying portions of the Ekman transport and entrainment in the stochastic forcing, are included [*Frankignoul*, 1985; *Dommenget and Latif*, 2002; *Lee et al.*, 2008].

2. The forcing and feedback are cyclostationary; that is, F and λ vary with the seasonal cycle [*Frankignoul*, 1985; *Ortiz and Ruiz de Elvira*, 1985; *Park et al.*, 2006].

3. The damping coefficient is given by $\lambda = \langle\lambda\rangle + \lambda'$, where $\langle\lambda\rangle$ is constant but λ' varies rapidly and can be approximated by white noise. As a result, there is a second, "multiplicative noise" term that depends upon the SST anomaly ($\lambda'T'_m$). Rapid fluctuations in λ', via wind gusts, can significantly contribute to the overall stochastic forcing [*Sura et al.*, 2006].

4. Air-sea feedback is enabled by using a second stochastic equation for surface air temperature, which is thermodynamically coupled to the ocean via the air-sea temperature difference [*Frankignoul*, 1985; *Barsugli and Battisti*, 1998]. With coupling, the air temperature adjusts to the underlying SSTA, reducing the thermal damping,
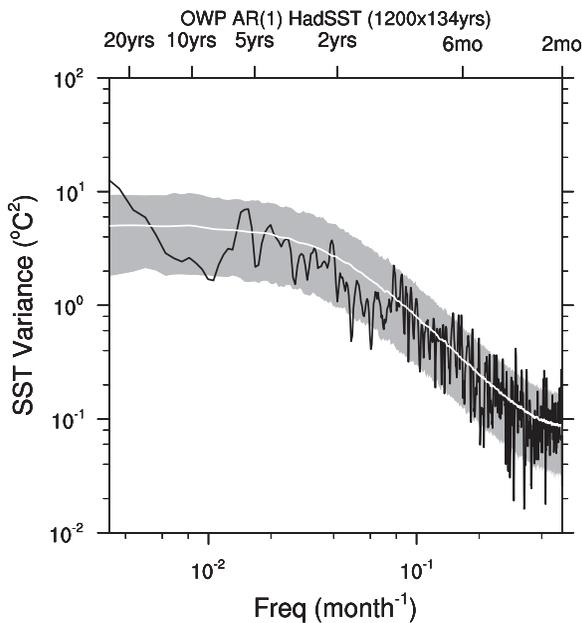
which significantly enhances the decadal SST variability but reduces the surface flux variability (it approaches zero at long time scales) and is apparent when comparing AGCMs with specified SSTs to those coupled to mixed

layer ocean models [*Bladé*, 1997; *Bhatt et al.*, 1998; *Saravanan*, 1998].

The primary effect of these extensions to the Hasselmann model is to increase the SSTA variance at annual and longer time scales.

4.2. Cloud-SST Feedbacks

Both the insolation and the amount of stratiform clouds are greatest over the North Pacific in summer. Increased clouds cool the ocean, while a colder ocean enhances the static stability, leading to more stratiform clouds that reduce Q_{sw} [*Norris and Leovy*, 1994; *Weare*, 1994; *Klein et al.*, 1995]. This positive feedback occurs over the central and western Pacific at ~40°N where there are strong gradients in both SST and cloud amount [*Norris et al.*, 1998]. The positive SST–low cloud feedback increases the persistence of North Pacific SST anomalies during the warm season [*Park et al.*, 2006].

4.3. "The Reemergence Mechanism"

Seasonal variations in h have the potential to influence the evolution of upper ocean thermal anomalies. *Namias and Born* [1970, 1974] were the first to note a tendency for midlatitude SST anomalies to recur from one winter to the next without persisting through the intervening summer. They speculated that temperature anomalies that form at the surface and spread throughout the deep winter mixed layer remain beneath the mixed layer when it shoals in spring. The thermal anomalies are then incorporated into the summer seasonal thermocline where they are insulated from surface fluxes that damp anomalies in the mixed layer. When h deepens again in the following fall, the anomalies are reentrained into the surface layer and influence the SST. *Alexander and Deser* [1995] termed this process the "reemergence mechanism" (shown schematically in Figure 3), and it has been documented over large portions of the North Atlantic and North Pacific oceans
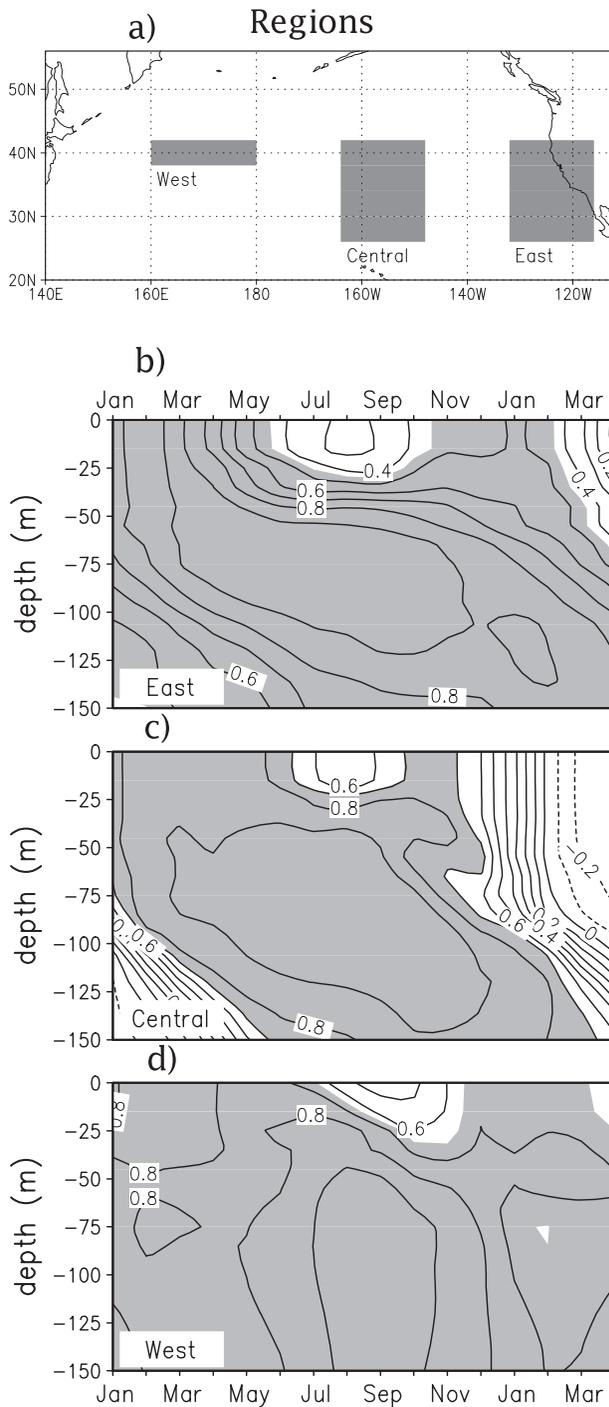
Figure 7. (opposite) (a) Pacific regions and reemergence mechanism as indicated by lead-lag regressions (°C (1°C)$^{-1}$) between temperature anomalies at 5 m in April–May and temperature anomalies from the previous January through the following April in the (b) east, (c) central, and (d) west Pacific regions. The contour interval is 0.1 and values greater than 0.55 (Figure 7b), 0.7 (Figure 7c), and 0.75 (Figure 7d) are shaded to highlight the reemergence mechanism. Computed using the National Centers for Environmental Prediction (NCEP) ocean assimilation analyses [*Ji et al.*, 1995]. Adapted from *Alexander et al.* [1999]. © American Meteorological Society. Reprinted with permission.

using subsurface temperature data and mixed layer model simulations [*Alexander et al.*, 1999, 2001; *Bhatt et al.*, 1998; *Watanabe and Kimoto*, 2000; *Timlin et al.*, 2002; *Hanawa and Sugimoto*, 2004].

The evolution of upper ocean temperatures in three North Pacific regions is shown by regressing the temperature anomalies as a function of month and depth on SST anomalies in April–May (Figure 7). The regressions depict how a 1°C SSTA in spring linearly evolves from the previous January through the following April. The regressions indicate the reemergence mechanism occurs in the east, central, and west Pacific: the anomalies that extend throughout the deep winter mixed layer are maintained beneath the surface in summer and then return to the surface in the following fall and winter. The regional differences in the timing and strength of the reemergence mechanism are partly due to variations in the seasonal cycle of *h* across the North Pacific. The maximum *h*, which tends to occur in March, increases from about 80 m along the west coast of North America to 120 m in the central Pacific and 150–250 m in the west Pacific (Figure 4).

Combining the Hasselmann model with one that includes the seasonal cycle of *h* significantly enhances the winter-to-winter autocorrelation of SST anomalies via the reemergence mechanism [*Alexander and Penland*, 1996; *Deser et al.*, 2003]. The lag autocorrelation of North Pacific SSTA starting from March indicates a clear annual cycle with peaks in March of successive years, due to the reemergence mechanism, while the total heat content (including the temperature anomalies in the summer thermocline) appears to decay at a constant rate, as expected from the Hasselmann model that uses the winter *h* to calculate the damping rate. This indicates that the winter mixed layer depth should be used when calculating the feedback parameter λ for studies of the year-to-year persistence of SST anomalies.

4.4. Dynamic Ocean Process

Ocean dynamics, including advection (term III), allows for additional mechanisms that contribute to SST variability on interannual and decadal times. Since currents advect ocean temperature anomalies, the reemergence process can be nonlocal; that is, SST anomalies created in one winter may return to the surface at a different location in the subsequent winter. Remote reemergence is pronounced in regions of strong currents such as the Gulf Stream [*de*
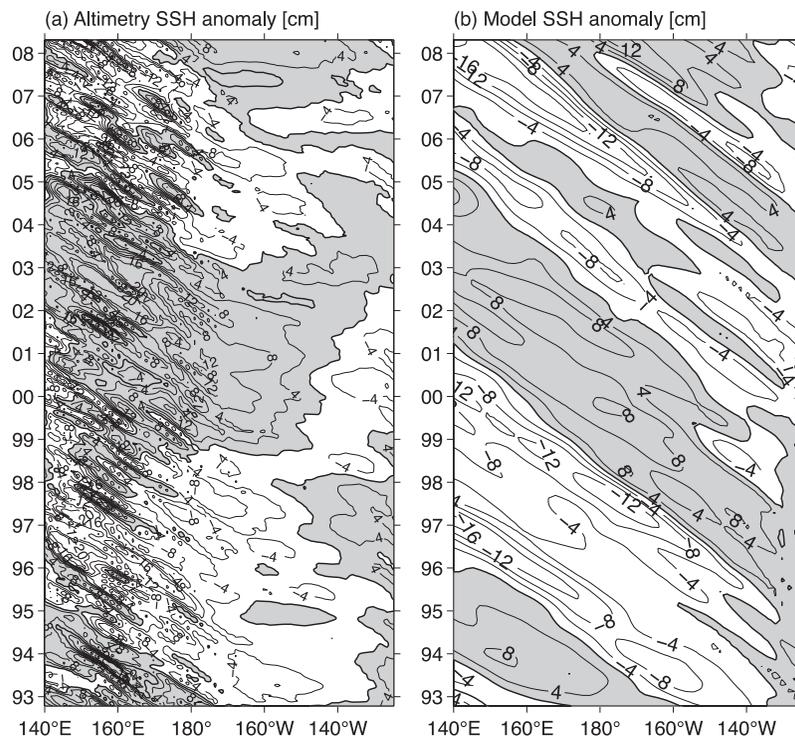

Figure 8. Sea surface height (SSH) anomalies along the zonal band of 32°–34°N from (a) the satellite altimeter data and (b) the wind-forced baroclinic Rossby wave model; see equation (5). Adapted from *Qiu et al.* [2007]. © American Meteorological Society. Reprinted with permission.

Coëtlogon and Frankignoul, 2003] and Kuroshio Extension [*Sugimoto and Hanawa*, 2005]. In the latter, anomalies created near Japan propagate to the central Pacific by the following winter.

Saravanan and McWilliams [1997, 1998] proposed the "advective resonance" hypothesis where a decadal SSTA peak can be generated based only on the spatial structure of atmospheric forcing and a constant ocean velocity. For interannual and longer periods, extratropical atmospheric variability tends to be dominated by fixed spatial patterns that are white in time. Stochastic forcing by these large-scale patterns can lead to low-frequency variability if the forcing has a multipole structure and the ocean advection traverses the centers of the poles. A simple model of such a system devised by Saravanan and McWilliams has two regimes, one where thermal damping dominates ocean advection and the other where advection dominates. In the former, the oceanic and atmospheric power spectra are slightly reddened but do not show any preferred periodicities. While in the latter, the overall variance in the atmosphere and ocean decreases, but a well-defined periodicity corresponding to the time scale emerges given by the length scale of the atmospheric forcing divided by the ocean velocity. *Wu and Liu* [2003] found that advective resonance could generate decadal variability in the eastern North Pacific, but the SST anomalies were initiated by Ekman transport rather than the net heat flux.

The dynamic adjustment of upper ocean gyre circulation primarily occurs via westward propagating Rossby waves forced by anomalous wind stress. The relevant equation for wind-forced waves can be written as [see *Dickinson*, 1978; *Gill*, 1982]

$$\frac{\partial h_t}{\partial t} + c\frac{\partial h_t}{\partial x} = \frac{1}{\rho_0 f}\nabla x\tau - \varepsilon h_t, \qquad (5)$$

where h_t is the depth of the thermocline, c is the speed of the first baroclinic mode Rossby wave, the constant ρ_0 is the seawater density, f is the Coriolis parameter, $\nabla x\tau$ is the wind stress curl that drives vertical motion via Ekman pumping, and ε is a damping coefficient. The h_t anomalies are generally compensated by perturbations in the sea surface height (SSH) [e.g., *Gill*, 1982], which can be measured via satellite [e.g., *Robinson*, 2004]. Rossby waves generated by large-scale wind forcing are long and thus nondispersive; that is, their speeds are independent of wavelength. The Rossby waves propagate nearly due west along a latitude circle (Figure 8), where c decreases rapidly with latitude. The large-scale Rossby wave response (Figure 8b) results from the integrated $\nabla x\tau$ forcing, producing maximum SSH (h_t) variability near the western boundary, while the full SSH field includes small-scale structures associated with eddies in the KE region

(Figure 8a). The dominant time scale of the large-scale response is set by the basin width, the spatial scale and location (relative to the western edge) of the atmospheric forcing, and the Rossby wave speed. At the latitude of the Kuroshio Extension (35°N), c is ~2.5 cm s^{-1}. For a basin the size of the Pacific, the adjustment time scale is on the order of ~5 (10) years if the Rossby wave was initiated in the central (far eastern) Pacific.

The Hasselmann model can also be used to understand the dynamical ocean response to wind forcing. Rossby waves excited by stochastic $\nabla x\tau$ forcing that is zonally uniform produce a h_t spectrum that increases with period but then reaches constant amplitude at low frequencies [*Frankignoul et al.*, 1997]. When the forcing has a more complex structure, such as sinusoidal waves in the zonal direction, decadal peaks can occur in the spectra because of resonance with the basin-scale Rossby waves [*Jin*, 1997], which is equivalent to the advective resonance mechanism but where the anomaly pattern propagates via Rossby waves rather than by the mean currents. Decadal peaks may also result from the reduction in Rossby wave speed as the latitude increases: wind forcing in the central Pacific creates westward Rossby waves that result in h_t anomalies of opposite sign on either side of the Kuroshio Current on ~10 year time scales [*Qiu*, 2003]. The gradient of h_t influences the strength of the jet via geostrophic adjustment.

The gyre adjustment process impacts SSTs through changes in thermocline depth and the currents. Given the westward deepening of the mixed layer across the basin between 30° and 50°N in winter (Figure 4), fluctuations in the upper thermocline are well below h in the central Pacific but close to the base of the mixed layer in the western Pacific. Thus, when Rossby waves propagate into the KE region in winter, the associated temperature anomalies can then be mixed to the surface via local turbulence. *Schneider and Miller* [2001] were thereby able to predict winter SSTA in the KE region several years in advance using the Rossby wave model (equation (5)), forced with the observed $\nabla x\tau$, plus a local linear regression between h_t and SST in the KE region. Anomalies in h_t and SST are relatively independent in the KE region in summer and over most of the North Pacific in all seasons.

Once the h_t anomalies propagate into the west Pacific, the position and strength of the KE changes [e.g., *Qiu*, 2000; *Kelly*, 2004; *Qiu and Chen*, 2005], which also impacts SSTs along ~40°N because of anomalous geostrophic heat transport [*Seager et al.*, 2001; *Schneider et al.*, 2002; *Dawe and Thompson*, 2007; *Kwon and Deser*, 2007; *Qiu et al.*, 2007]. Satellite altimetry data and high-resolution ocean models indicate that the large-scale flow resulting from the arrival
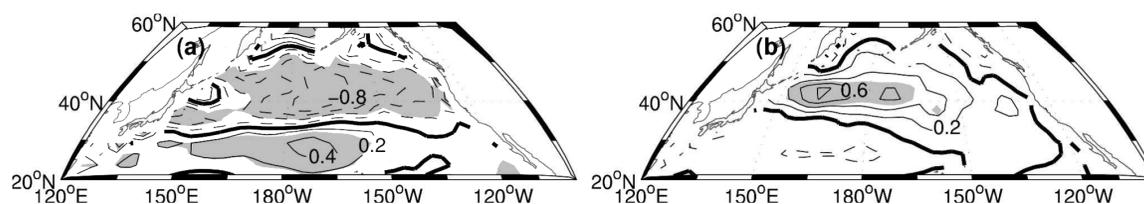
Figure 9. Atmospheric (a) forcing and (b) response to SST anomalies in the Kuroshio Extension region. Regression of wind stress curl anomalies on the winter-normalized SST anomalies in the KE region (35°–45°N, 140°E–180°) is shown. Annual mean wind stress curl leads SST index by 4 years; both variables are smoothed with a 10 year low-pass filter (Figure 9a). Annual mean wind stress curl lags the SST index by 1 year based on unfiltered data (Figure 9b). The unfiltered regression pattern is further scaled by the ratio of the standard deviation of 10 year low-pass-filtered SST index to that of unfiltered SST index. Contour intervals are 0.2×10^{-8} N m^{-3}. Negative values are dashed, and shading indicates regressions significant at 99%. Results are from a long coupled NCAR GCM simulation. Adapted from *Kwon and Deser* [2007]. © American Meteorological Society. Reprinted with permission.

of Rossby waves affects the strength of the front and eddy activity in the KE region [*Qiu and Chen*, 2005; *Taguchi et al.*, 2005, 2007], where the resulting ageostrophic currents influence SSTA [*Dawe and Thompson*, 2007].

4.5. Midlatitude Air-Sea Interaction

While atmospheric forcing was crucial in generating low-frequency variability in the aforementioned studies, they did not require an atmospheric response to the developing ocean anomalies. Coupled feedbacks could enhance or give rise to new midlatitude modes of decadal variability. On the

basis of analyses of a coupled atmosphere ocean GCM, *Latif and Barnett* [1994, 1996] proposed a feedback loop between the strength of the Aleutian Low and the subtropical ocean gyre circulation to account for the presence of decadal oscillations. They argued that an intensification of the Aleutian Low would strengthen the subtropical gyre after a delay associated with the Rossby wave adjustment process. An anomalously strong subtropical gyre transports more warm water into the Kuroshio Extension, leading to positive SST anomalies in the western and central North Pacific. In their coupled model experiment and in supplementary AGCM simulations with prescribed SSTA, the
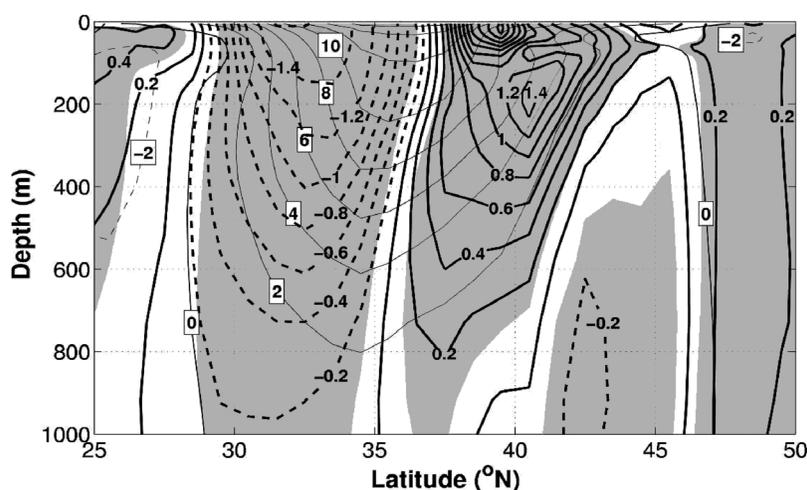

Figure 10. Relationship between temperature anomalies in the Kuroshio Extension and changes in the ocean gyres. Simultaneous regression of (December-January-February-March (DJFM) subsurface zonal current velocity along 150°E on the SST anomalies are averaged over the KE region. Both variables have been low-pass filtered to retain periods longer than 10 years. Contour interval is 0.2 cm s^{-1} °C^{-1}, and the shading indicates regressions significant at 99%. Solid (dashed) contours denote eastward (westward) velocity. Thin contours with boxed labels indicate the climatological winter (DJFM) mean zonal velocity fields. Contour interval for the mean zonal velocity is 2 cm s^{-1}. Results are from a long coupled NCAR GCM simulation [*Kwon and Deser*, 2007]. © American Meteorological Society. Reprinted with permission.

atmosphere was very sensitive to SST variations in the KE region, where a strong anomalous high developed over the central Pacific in response to positive SST anomalies in the KE. The circulation around the high advected warm moist air over the positive SSTA, which maintained the SST anomalies but reduced the strength of the Aleutian Low, which subsequently weakened the subtropical gyre, switching the phase of the oscillation about 10 years later.

While many aspects of the *Latif and Barnett* [1994, 1996] hypothesis occur in nature, such as the Rossby wave adjustment to $\nabla x\tau$ anomalies associated with the strength of the Aleutian Low, some are not consistent with data and ocean model simulations driven by observed atmospheric conditions. In particular, when the Aleutian Low strengthens, it also shifts southward; as a result, the gyre circulation shifts equatorward, and the SST anomalies subsequently cool rather than warm in the KE region (Figure 9) [*Deser et al.*, 1999; *Miller and Schneider*, 2000; *Seager et al.*, 2001], as discussed further in section 5.2.3. In addition, rather than a positive thermal air-sea feedback, surface heat fluxes damp SST anomalies in the KE region both in observations and ocean model hindcasts [*Seager et al.*, 2001; *Tanimoto et al.*, 2003; *Kelly*, 2004]. Finally, the atmospheric response in the AGCM simulations conducted by Latif and Barnett were much larger than in nearly all other AGCM experiments [see *Kushnir et al.*, 2002].

While the original Latif and Barnett mechanism may not be fully realized, midlatitude ocean-to-atmosphere feedbacks still appear to influence decadal variability. Observations, theoretical models, and coupled GCMs suggest there is positive air-sea feedback in the North Pacific [*Weng and Neelin*, 1999; *Schneider et al.*, 2002; *Wu etal.*, 2005; *Kwon and Deser*, 2007; *Frankignoul and Sennéchael*, 2007; *Qiu et al.*, 2007]. As in the original Latif and Barnett hypothesis, wind stress curl anomalies in the central Pacific generate ocean Rossby waves that lead to adjustment of the ocean gyres ~5 years later (Figure 9a), but in contrast to Latif and Barnett, the SST anomalies in the Kuroshio region are maintained by geostrophic currents because of a change in the position of the gyre (Figure 10) and to some extent the Ekman transport rather than surface fluxes. When the gyres shift north, KE SSTs increase, and the upward directed latent heat fluxes lead to enhanced precipitation over the KE region and, in some model experiments, a broader atmospheric response that includes $\nabla x\tau$ anomalies over the central North Pacific that are similar in structure but opposite in sign and somewhat weaker than the curl anomalies, reversing the sign of the oscillation forcing pattern (Figure 9b). While this coupled feedback loop explains a small amount of the overall SST variance, it produces a modest spectral peak above the red noise background on

decadal time scales [*Kwon and Deser*, 2007; *Qiu et al.*, 2007].

4.6. Tropical-Extratropical Interactions

Variability in the North Pacific may not only be generated by extratropical processes but may also arise because of fluctuations originating in the tropics that are communicated to midlatitudes by the atmosphere and/or ocean. Furthermore, two-way interactions between the tropical and North Pacific may impact low-frequency variability in both domains.

4.6.1. "The Atmospheric Bridge" (ENSO teleconnections). ENSO-driven atmospheric teleconnections [*Trenberth et al.*, 1998; *Liu and Alexander*, 2007; *Nakamura et al.*, this volume] alter the near-surface air temperature, humidity, wind, and clouds far from the equatorial Pacific. The resulting variations in the surface heat, momentum, and freshwater fluxes cause changes in SST, *h*, salinity, and ocean currents. Thus, the atmosphere acts like a bridge spanning from the equatorial Pacific to the North Pacific, South Pacific, the North Atlantic, and Indian oceans [e.g., *Alexander*, 1990, 1992a; *Lau and Nath*, 1994, 1996, 2001; *Klein et al.*, 1999; *Alexander et al.*, 2002]. The SST anomalies that develop in response to this "atmospheric bridge" may feed back on the original atmospheric response to ENSO.

When El Niño events peak in boreal winter, enhanced cyclonic circulation around the deepened Aleutian Low (Plate 1a) results in anomalous northwesterly winds that advect relatively cold dry air over the western/central North Pacific, anomalous southerly winds that advect warm moist air along the west coast of North America, and enhanced surface westerlies over the central North Pacific. The resulting anomalous surface heat fluxes and Ekman transport create negative SSTA between 30°N and 50°N west of ~150°W and positive SSTA along the west coast of North America (Plate 1a) [*Alexander et al.*, 2002; *Alexander and Scott*, 2008]. In the central North Pacific, the stronger wind stirring and negative buoyancy forcing due to surface cooling increases the *h* through the winter, and some of the anomalously cold water returns to the surface in the following fall/winter via the reemergence mechanism [*Alexander et al.*, 2002].

Studies using AGCM mixed layer ocean model simulations have confirmed the basic bridge hypothesis for forcing North Pacific SST anomalies but have reached different conclusion on the impact of these anomalies on the atmosphere [*Alexander*, 1992b; *Bladé*, 1999; *Lau and Nath*, 1996, 2001]. More recent model experiments suggest that the oceanic feedback on the extratropical response to ENSO is complex but of modest amplitude; that is, atmosphere-ocean
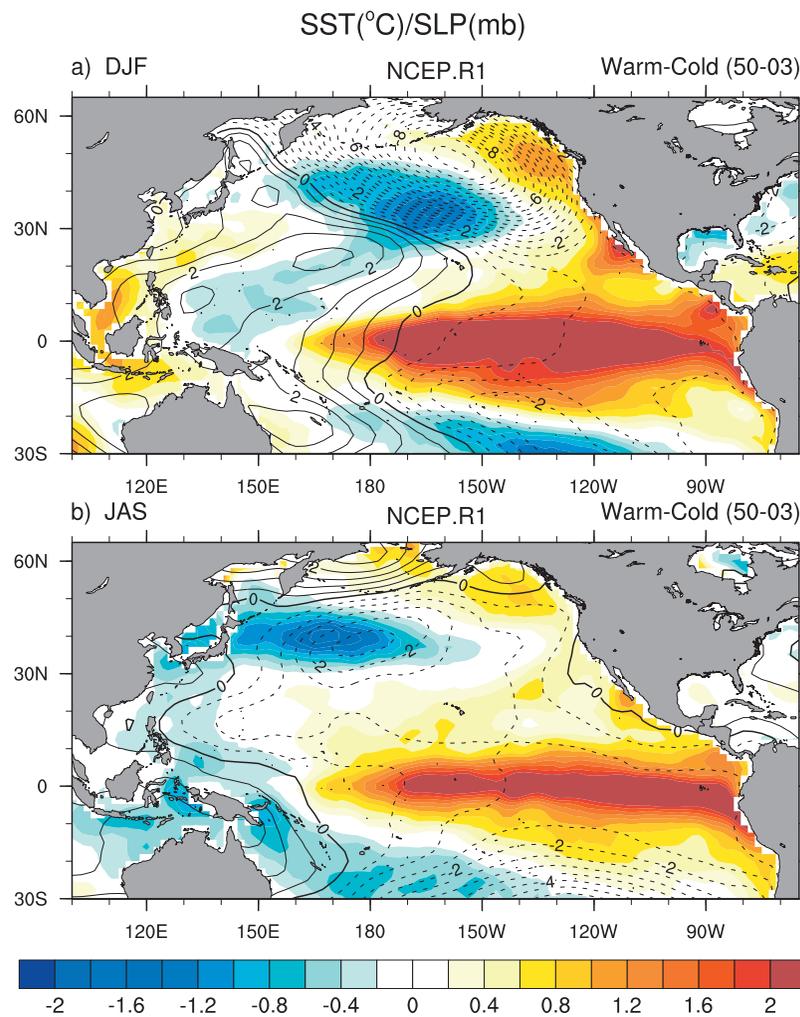
SST(°C)/SLP(mb)

Plate 1. ENSO signal including the atmospheric bridge as indicated by the composite of 10 El Niño minus 10 La Niña events for SLP (contours, interval 0.5 mbar) and SST (shading, interval 0.2°C) during (a) DJF when ENSO peaks and (b) the previous July-August-September (JAS). The fields are obtained from NCEP atmospheric reanalysis [*Kalnay et al.*, 1996; *Kistler et al.*, 2001].

coupling outside of the tropical Pacific slightly modifies the extratropical atmospheric circulation anomalies, but these modifications depend on the seasonal cycle and air-sea interactions both within and beyond the North Pacific Ocean [*Alexander et al.*, 2002; *Alexander and Scott*, 2008].

Most studies of the atmospheric bridge have focused on boreal winter since ENSO and the associated atmospheric circulation anomalies peak at this time. However, significant bridge-related changes in the climate system also occur in other seasons. Over the western North Pacific, the southward displacement of the jet stream and storm track in the summer prior to when ENSO peaks changes the solar radiation and latent heat flux at the surface, which results in

anomalous cooling and deepening of the oceanic mixed layer at ~40°N [*Alexander et al.*, 2004; *Park and Leovy*, 2004]. The strong surface flux forcing in conjunction with the relatively thin mixed layer in summer leads to the rapid formation of large-amplitude SST anomalies in the Kuroshio Extension (Plate 1b).

While the atmospheric bridge primarily extends from the tropics to the extratropics, variability originating in the North Pacific may also influence the tropical Pacific. *Barnett et al.* [1999] and *Pierce et al.* [2000] proposed that the atmospheric response to slowly varying SST anomalies in the Kuroshio Extension region extends into the tropics, thereby affecting the trade winds and decadal variability

in the ENSO region. *Vimont et al.* [2001, 2003] found that the extratropical atmosphere can generate tropical variability via the "seasonal footprinting mechanism." Large fluctuations in the North Pacific Oscillation, an intrinsic mode of atmospheric variability, impart an SST footprint onto the ocean during winter via changes in the surface heat fluxes, which persists through summer in the subtropics and impacts the atmospheric circulation including zonal wind stress anomalies that extend onto and south of the equator. These wind stress anomalies are an important element of the stochastic forcing of interannual and decadal ENSO variability [*Vimont et al.*, 2003; *Alexander et al.*, 2008].

4.6.2. Ocean teleconnections. The equatorial thermocline variability associated with ENSO excites Kelvin and other coastally trapped ocean waves, which propagate poleward along the eastern Pacific boundary in both hemispheres, generating substantial sea level variability [*Enfield and Allen*, 1980; *Chelton and Davis*, 1982; *Clarke and van Gorder*, 1994]. However, these waves impact the ocean only within ~50 km of shore north of 15°N [*Gill*, 1982]. Energy from the coastal waves can also be refracted as long Rossby waves that propagate westward across the extratropical Pacific [*Jacobs et al.*, 1994; *Meyers et al.*, 1996]. However, wind forcing rather than the eastern boundary waves appears to be the dominant source of Rossby waves across much of the North Pacific [*Miller et al.*, 1997; *Chelton and Schlax*, 1996; *Fu and Qiu*, 2002].

Gu and Philander [1997] proposed a mechanism for decadal variability that relies on the subduction of surface temperature anomalies in the North Pacific and their subsequent southward propagation in the lower branch of the STC. Upon reaching the equator, the thermal anomalies upwell to the surface and amplify via interactions between the zonal wind, SST gradient, and upwelling, known as the "Bjerknes feedback" [e.g., see *Neelin et al.*, 1998], and subsequently influence the North Pacific via the atmospheric bridge. If warm water is subducted, the subsequent
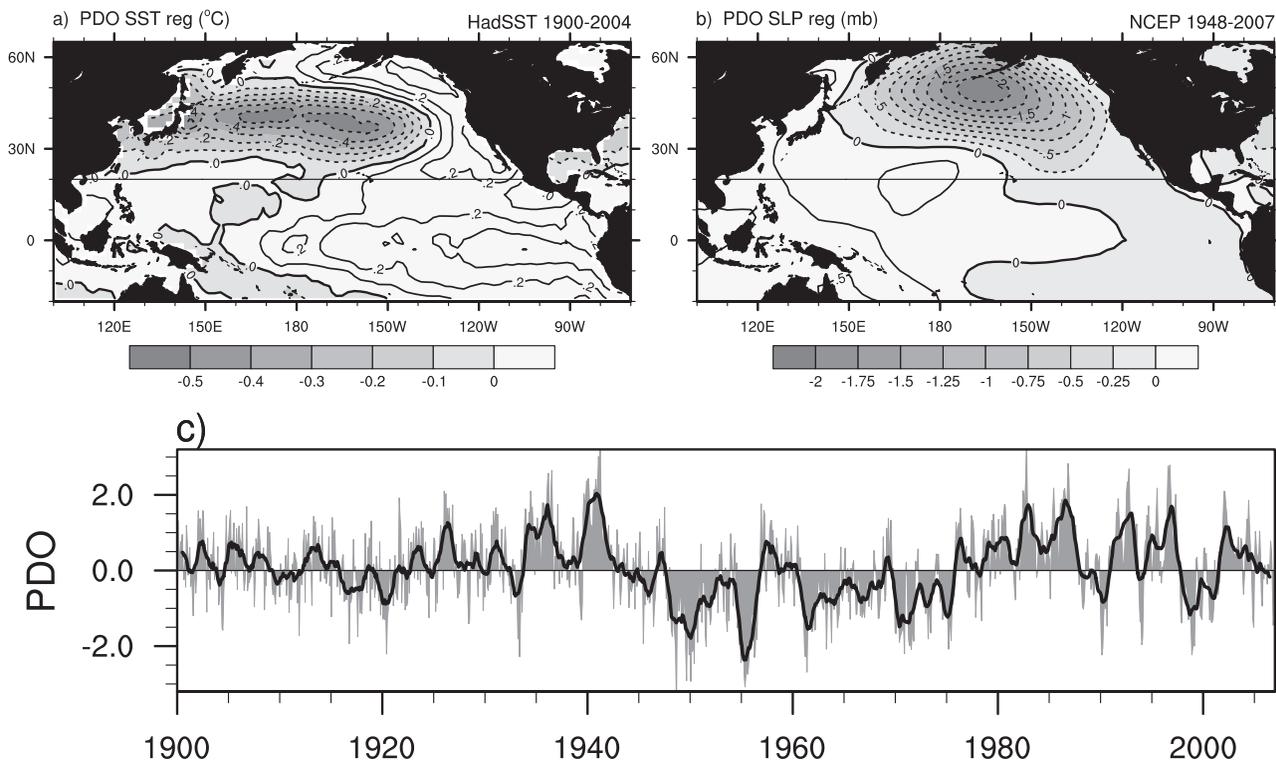

Figure 11. Pacific Decadal Oscillation spatial and temporal structure: the leading pattern SST and SLP anomalies north of 20°N and normalized time series of monthly SST anomalies (PDO index, defined by *Mantua et al.* [1997]). Regressions of the PDO index on the (a) observed SST (contour interval (CI) 0.1°C per 1σ PDO value) and (b) SLP (CI 0.25 mbar per 1σ PDO value). The SSTs were obtained from the HadSST data set for the period 1900–2004, and the SLP values were obtained from NCEP reanalysis for the years 1948–2007. (c) Monthly PDO index (gray shading) and 12 month running mean (black line) during 1900–2007, obtained from http://jisao.washington.edu/pdo/PDO.latest.

positive anomalies on the equator will act to strengthen the Aleutian Low, which creates cold anomalies in the central North Pacific (Plate 1). This describes one-half of the oscillation, the period of which is controlled by the time it takes the water parcels to travel from the surface in the extratropics to the equator. While observations show evidence of thermal anomalies subducting in the main thermocline in the central North Pacific [*Deser et al.*, 1996; *Schneider et al.*, 1999], these anomalies decay away from the subduction region, and the thermocline variability found equatorward of 18° appears to be primarily associated with tropical wind forcing [*Schneider et al.*, 1999; *Capotondi et al.*, 2003]. SSTs in the equatorial Pacific, however, may still be influenced by subduction and transport from the South Pacific [*Luo and Yamagata*, 2001].

An alternate subduction-related hypothesis is that changes in the subtropical winds alter the speed of the STC, thus changing the rate at which relatively cold water from the surface layer in the extratropics is transported southward and then upwells at the equator. Using an atmosphere-ocean model of intermediate complexity, *Kleeman et al.* [1999] found that decadal variations of tropical SSTs could be induced by changes in the subtropical winds, while the observational analyses of *McPhaden and Zhang* [2002] indicated that slowing of the STCs in both hemispheres after 1970 relative to the previous two decades reduced upwelling along the equator and resulted in substantially warmer SSTs in the central equatorial Pacific.

4.6.3. Two-way connections. Liu et al. [2002] and *Wu et al.* [2003] performed sensitivity experiments using "model surgery" in which ocean-atmosphere interaction can be turned on and off in different regions. These experiments suggest that decadal variability arises in the tropical and North Pacific via independent mechanisms, but variability in both basins can be enhanced by tropical-extratropical interactions. For example, tropical Pacific decadal SST variance is almost doubled when extratropical ocean-atmosphere interaction and oceanic teleconnections are enabled. Observational [*Newman*, 2007] and modeling studies [*Solomon et al.*, 2003, 2008] support the concept of two-way coupling where variability in the North Pacific influences tropical low-frequency variability and vice versa.

5. PACIFIC DECADAL OSCILLATION

5.1. Pattern and Temporal Variability

The leading pattern of North Pacific monthly SST variability, as identified by empirical orthogonal function (EOF) analysis and the corresponding principal component (PC 1), the time series of the amplitude and phase of EOF 1, is shown in Figure 11. The time series (after removing the global mean temperature) has been termed the Pacific Decadal Oscillation by *Mantua et al.* [1997] because of its low-frequency fluctuations. The PDO underwent rapid transitions between relatively stable states or "regime changes" around 1925, 1947, and 1976, although interannual variability is also apparent in the PDO time series. In the North Pacific, the PDO pattern has anomalies of one sign in the central and western North Pacific between approximately 25° and 45°N that are ringed by anomalies of the opposite sign. However, the associated SST anomalies extend over the entire basin and are symmetric about the equator [*Zhang et al.*, 1997; *Garreaud and Battisti*, 1999], leading some to term the phenomenon the Interdecadal Pacific Oscillation [*Power et al.*, 1999; *Folland et al.*, 2002].

The decadal SST transitions were accompanied by widespread changes in the atmosphere, ocean, and marine ecosystems [e.g., *Miller et al.*, 1994; *Trenberth and Hurrell*, 1994; *Benson and Trites*, 2002; *Deser et al.*, 2004]. For example, *Mantua et al.* [1997] found that timing of changes in the PDO closely corresponded to those in salmon production along the west coast of North America. The positive phase of the PDO, with cold water in the central Pacific and warm water along the coast of North America, is accompanied by a deeper Aleutian Low, with negative sea level pressure (SLP) anomalies over much of the North Pacific (Figure 11), warm surface air temperature over western North America, enhanced precipitation over Alaska and the southern United States, and reduced precipitation across the northern United States/southern Canada [*Mantua et al.*, 1997; *Deser et al.*, 2004].

5.2. Mechanisms for the PDO

The PDO could be a critical factor in long-range forecasts given its long time scale and connection to many important climatic and biological variables. However, this depends on whether the mechanism(s) underlying the PDO is (are) predictable and the relationship between PDO SSTA and the associated large-scale atmospheric circulation. That is, is the PDO (1) driving, (2) responding to, or (3) coupled with the later? We will expand on the processes underlying midlatitude SST variability discussed in section 4 as potential mechanisms for the PDO.

5.2.1. Fluctuations in the Aleutian Low (large-scale stochastic forcing). The Hasselmann model for SSTs at a given location can be extended to understand basin-wide SST anomaly patterns. *Frankignoul and Reynolds* [1983]

found that white noise forcing associated with large-scale atmospheric fluctuations could explain much of the variability over the entire North Pacific, while *Cayan* [1992b] and *Iwasaka and Wallace* [1995] found that interannual variability in the surface fluxes and SSTs is closely linked to the dominant patterns of atmospheric circulation over the North Pacific and North Atlantic oceans. We explore SLP/Q_{net}/SST relationships using an AGCM coupled to a variable depth ocean mixed layer model (MLM), with no ocean currents and hence no ENSO variability or ocean gyre dynamics. As in nature, the leading pattern of SLP variability over the North Pacific is associated with fluctuations in the Aleutian Low (Figure 12a). The near-surface circulation around a stronger low results in enhanced wind speeds and reduced air temperature and humidity along ~35°N, which cools the underlying ocean via the surface heat fluxes, while the northward advection of warm moist air heats the ocean near North America. The structure of the SLP-related surface flux anomalies (Figure 12b) is very similar to the dominant surface flux and SST patterns (Figures 12c and 12d). Given that the model has no ocean currents and similar SLP and flux patterns are found in AGCM simulations with climatological SSTs as boundary conditions [*Alexander and Scott*, 1997], fluctuations in the Aleutian Low can drive PDO-like SST anomalies via the surface flux field.
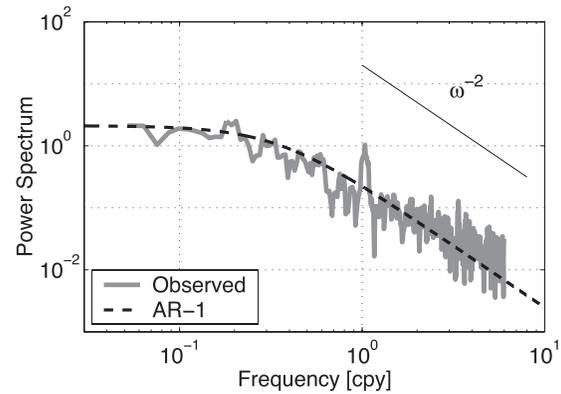

Figure 13. Power spectrum of the observed PDO index. Dashed line indicates the best fit based on a first-order autoregressive model; thin solid line shows the theoretical slope for intermediate frequency portion of the spectrum from a stochastic model. Adapted from *Qiu et al.* [2007]. © American Meteorological Society. Reprinted with permission.

The temporal characteristics of the PDO are also consistent with the Hasselmann model; that is, it exhibits a red noise spectrum without significant spectral peaks other than at the annual period (Figure 13). *Pierce* [2001] generated 100 year synthetic time series using a random number
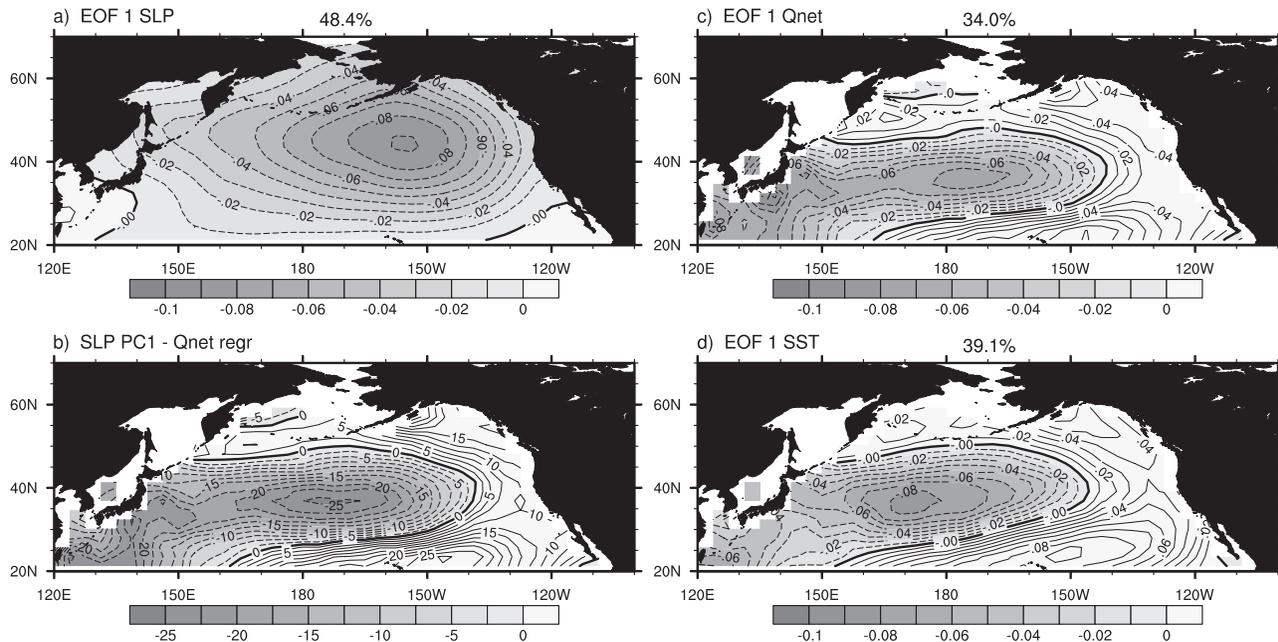

Figure 12. SLP, flux, and SST anomaly patterns associated with the Aleutian Low during winter (DJF). (a) EOF 1 of SLP, regression values of the local (b) Q_{net} (contour interval 2.5 W m^{-2}) and (c) SST (CI is 0.05°C) anomalies on PC1 of SLP, and (d) EOF 1 of SST. All fields are obtained from a 50 year simulation of the Geophysical Fluid Dynamics Laboratory (GFDL) AGCM coupled to an ocean MLM over the ice-free ocean.

generator and the same lag one autocorrelation coefficient as the observed PDO. The synthetic time series exhibited similar low-frequency variability as the observed PDO with strings of years of the same sign separated by abrupt "regime shifts" and exhibiting "significant" (at the 95% level) spectral peaks but at different periods. These findings suggest caution in attributing physical meaning to regime shifts and spectral peaks even in century-long data sets.

5.2.2. Teleconnections from the tropics. Mantua et al. [1997] noted that the PDO had only a modest correlation with ENSO and that the North Pacific variability was of greater amplitude and lower frequency than that in the tropical Pacific. However, the atmospheric bridge to the North Pacific is complex and is a function of season, lag, and location [*Newman et al.*, 2003] and also depends on the ENSO index, data set, etc. [*Alexander et al.*, 2008]. Furthermore, the ENSO-related North Pacific SST anomaly pattern during winter (Plate 1a) clearly resembles the PDO, while the summer ENSO signal (Plate 1b) also projects on the PDO pattern, particularly in the western North Pacific. So, to what extent do ENSO and tropical SSTs in general impact the PDO?

Zhang et al. [1997] utilized several analysis techniques to separate interannual ENSO variability from a residual containing the remaining (>7 years) "interdecadal" variability.
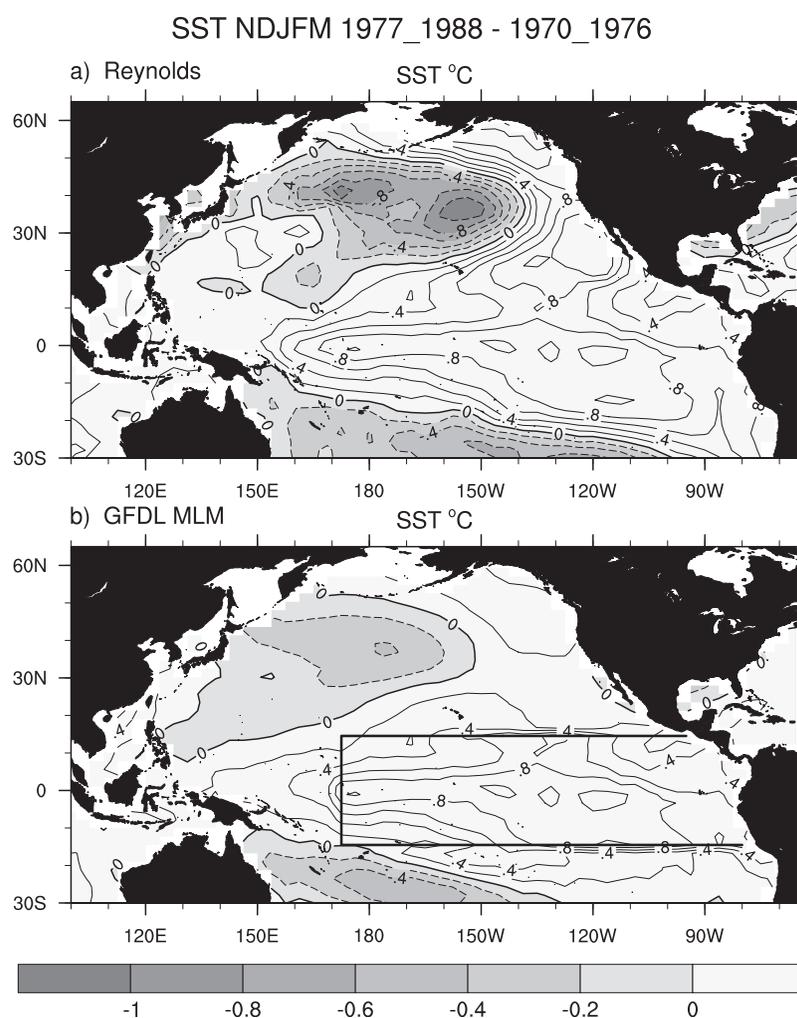

Figure 14. The 1977–1988 minus the 1970–1976 average SST during November-December-January-February-March (NDJFM) from (a) observations and (b) an ensemble average of 16 model simulations. The observations and model integrations are described by *Smith et al.* [1996] and *Alexander et al.* [2002], respectively. The model consists of an AGCM coupled to an ocean mixed layer ocean model over the ice-free global oceans except in the central/eastern tropical Pacific (box) where observed SSTs are specified. Negative values are shaded, and the CI is 0.2°C.

The SSTA pattern based on low-pass-filtered data is similar to the unfiltered ENSO pattern, except it is broader in scale in the eastern equatorial Pacific and has enhanced magnitude in the North Pacific relative to the tropics. The extratropical component closely resembles the PDO. Other statistical methods of decomposing the data indicate that at least a portion of the decadal variability in the PDO region is associated with anomalies in the tropical Pacific [e.g., *Nakamura et al.*, 1997; *Mestas Nuñez and Enfield*, 1999; *Alexander et al.*, 2008].

While the broad structure of the first EOF of SSTA in observations (Figure 11a) and the AGCM-MLM (Figure 12d) are similar, the anomalies extend along ~40°N in nature but slope southwestward from the central Pacific toward the South China Sea in the model. This bias could be due to several factors, including the absence of ENSO/the atmospheric bridge in the original AGCM-MLM simulations. In AGCM-MLM–tropical Pacific_observation (TP_OBS) experiments, in which the MLM is coupled to the AGCM except in the tropical Pacific where observed SSTs are prescribed for the years 1950–1999, the dominant pattern of North Pacific SSTAs closely resembles the observed PDO [see *Alexander et al.*, 2002, Figure 5].

The observed difference between SSTs averaged over periods 1977–1988 and 1970–1976 during winter includes warm ENSO-like conditions in the tropical Pacific and the positive phase of the PDO in the North Pacific (Figure 14a). A comparable plot based on an ensemble average of 16 AGCM-MLM-TP_OBS simulations has a similar pattern in the North Pacific (Figure 14b), confirming that the atmospheric bridge can contribute to low-frequency variability in the PDO, although the amplitudes of the North Pacific anomalies in the MLM are ~1/3 of their observed counterparts. While there is a wide range in epoch differences between ensemble members (not shown), this estimate of ENSO's impact on low-frequency PDO variability is consistent with that of *Schneider and Cornuelle* [2005], discussed later in this section.

The influence of the tropics on decadal variability in the North Pacific via the atmospheric bridge may occur via the teleconnection of decadal signals originating in the ENSO region [*Trenberth*, 1990; *Graham et al.*, 1994; *Deser and Phillips*, 2006], decadal forcing from other portions of the tropical Pacific and Indian oceans [*Deser et al.*, 2004; *Newman*, 2007], and/or ENSO-related forcing on interannual time scales, which is integrated or reddened by ocean
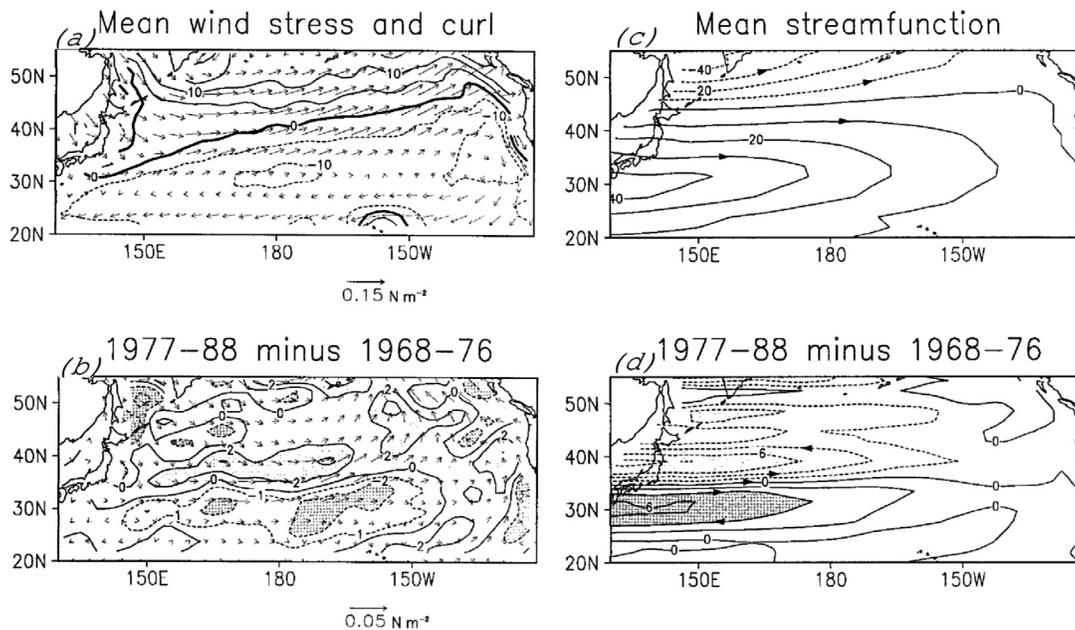

Figure 15. Annual (a) long-term mean and (b) 1977–1988 minus 1968–1976 wind stress (vectors) and its curl (contours) from the NCEP reanalysis. The CI is 5×10^{-8} N m^{-3} in Figure 15a and 2×10^{-8} N m^{-3} in Figure 15b where the -1×10^{-8} N m^{-3} contour is also shown and values $<-2 \times 10^{-8}$ N m^{-3} are shaded. Annual (c) long-term mean and (d) 1977–1988 minus 1968–1976 geostrophic transport stream function, given by the Sverdrup minus Ekman currents: the adjusted ocean circulation to wind curl forcing. The CI is 10 Sv in Figure 15c and 2 Sv in Figure 15d where values >4 Sv are shaded. Adapted from *Deser et al.* [1999]. © American Meteorological Society. Reprinted with permission.

processes in the North Pacific, including the reemergence mechanism [*Newman et al.*, 2003; *Schneider and Cornuelle*, 2005]. *Alexander et al.* [1999, 2001] showed that the PDO pattern could recur in consecutive winters via the reemergence mechanism.

5.2.3. Midlatitude ocean dynamics and coupled variability. The role of ocean dynamics in PDO variability has been investigated through the change in ocean circulation that occurred in 1976–1977, when the ocean rapidly transitioned from the negative to positive phase of the oscillation (Figure 11c). The strengthening and southward displacement of the Aleutian Low beginning in the winter of 1976 and in the decade that followed cooled the central Pacific by enhanced Ekman transport, vertical mixing, and upward surface heat flux [*Miller et al.*, 1994]. This cooling projected strongly on the PDO in the center of the basin. In addition, the maximum westerly winds intensified and

shifted from about 40°N to 35°N, and hence $\nabla x\tau$ and Ekman pumping shifted southward, with anomalous downward (upward) values south (north) of 35°N (Figures 15a and 15b). Following the Rossby waves adjustment process to the wind forcing (see section 4.4), the thermocline deepened (shoaled) south (north) of the mean KE axis at ~35°N, and the gyres strengthened and shifted southward over an ~5 year period (Figures 15c and 15d). Geostrophic advection associated with southward gyre position strongly cooled the ocean along 40°N. The SST anomalies in the KE region also project onto the PDO, helping to maintain the positive phase of the PDO through the 1980s.

The 20–30 year persistence of anomalies in the PDO record and ~15–25 year period of PDO variability in paleoclimate reconstructions [*Biondi et al.*, 2001; *Gedalof*, 2002] and in some coupled GCM studies has led some to suggest that the PDO is due to positive atmosphere-ocean feedbacks necessary to sustain decadal oscillations. While
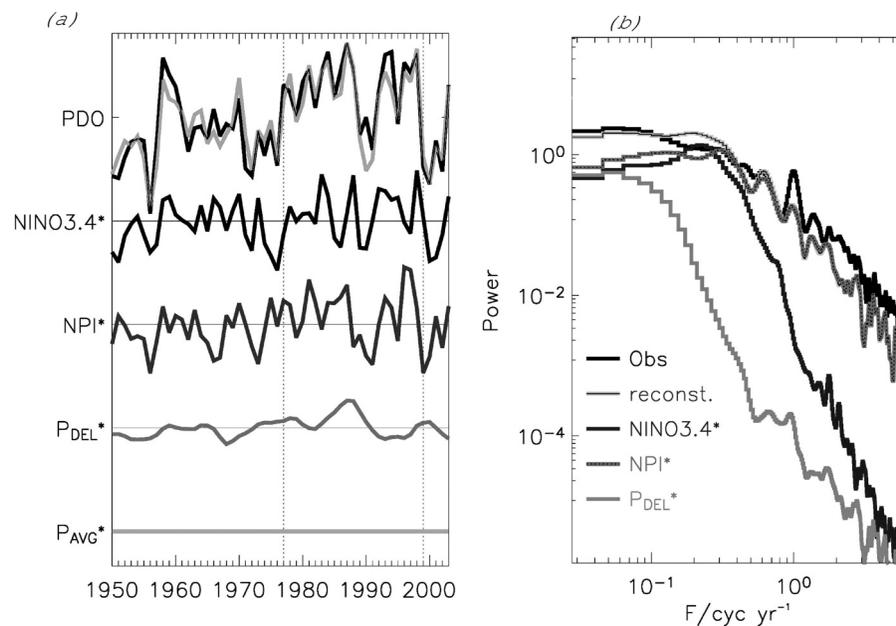

Figure 16. (a) PDO time series and reconstruction (gray) based on contributions to the PDO from ENSO teleconnections (Niño 3.4*), stochastic fluctuations in the Aleutian Low indicated by the North Pacific index (NPI*), and the change in the ocean gyres given by the difference in the zonal average ocean pressure difference (P^*_{DEL}) (indicative of the slope of the thermocline and hence the strength/position of the ocean gyres) between 38° and 40°N in the KE region. The asterisk indicates that the mutual variance between the forcing indices has been subtracted using regression analysis. The index for thermocline depth estimate from 35° to 38°N in the KE region (P^*_{AVG}) does not explain a significant fraction of the SSTA variability of the PDO. Dotted vertical lines mark the winters of 1976/1977 and 1998/1999. (b) Power spectrum of the observed and reconstructed PDO and contributions resulting from the NPI*, Niño 3.4*, and P^*_{DEL}. Spectra have been smoothed by three successive applications of a five-point running mean. Note the dominance of the NPI* and ENSO* contributions to the PDO at internal annual time scales and the roughly equal contribution of the three factors at decadal time scales. From *Schneider and Cornuelle* [2005]. © American Meteorological Society. Reprinted with permission.

the North Pacific Ocean appears to have the necessary dynamics to generate low-frequency variability, it is unclear whether the atmospheric response to the associated SST anomalies has the correct spatial pattern, phase, and amplitude for decadal oscillations. On one hand, recent coupled GCM experiments [Kwon and Deser, 2007] and observationally derived heuristic models [Qiu et al., 2007] suggest that the atmospheric response to SST anomalies in the Kuroshio Extension region, while modest, is sufficiently strong to enhance variability at decadal periods. On the other hand, the wind stress curl pattern diagnosed as the response to the KE SST anomalies by Kwon and Deser [2007] was of one sign across the Pacific at ~40°N, while Qiu et al. [2007] found that it switched signs in the center of the basin. There are also conflicting results from AGCM studies with either specified SST anomalies [e.g., Peng et al., 1997; Peng and Whitaker, 1999] or where the ocean component is a slab mixed layer and an anomalous heat source, representing geostrophic heat flux convergence, is added in the KE region [Yulaeva et al., 2001; Liu and Wu, 2004; Kwon and Deser, 2007]. Some models exhibit a baroclinic response with a surface low that decreases with height downstream over the central Pacific, while others have an equivalent barotropic response with a surface high that increases with height over the central Pacific. The former is in direct response to the low-level heating, while the latter is stronger and driven by changes in the storm track. In addition, most AGCM studies have found that the response to extratropical SSTs is relatively small compared to internal atmospheric variability [Kushnir et al., 2002], although the current generation of coupled GCMs may not sufficiently resolve all of the oceanic as well as atmospheric processes that could contribute to the PDO.

5.2.4. PDO: A multiprocess phenomena?. How can we reconcile these conflicting findings on the mechanism for the PDO? Several recent studies have used statistical analyses to reconstruct the annually averaged (July–June) PDO and to determine the processes that underlie its dynamics. Newman et al. [2003] found that the PDO is well modeled as the sum of atmospheric forcing represented by white noise, forcing due to ENSO, and memory of SST anomalies in the previous year via the reemergence mechanism. Expanding on this concept, Schneider and Cornuelle [2005] found that the annually averaged PDO could be reconstructed based on an AR1 model and forcing associated with stochastic variability in the Aleutian Low, ENSO teleconnections, and shifts in the North Pacific Ocean gyres; vertical mixing of temperature anomalies associated with wind-driven Rossby waves had little impact on the

PDO (Figure 16a). On interannual time scales, random Aleutian Low fluctuations and ENSO teleconnections were about equally important in determining the PDO variability with negligible contributions from ocean currents, while on decadal time scales, stochastic forcing, ENSO, and changes in the gyre circulations each contributed approximately 1/3 of the PDO variance (Figure 16b). A key implication of these analyses is that, unlike ENSO, the PDO is likely not a single physical mode but rather the sum of several phenomena. Furthermore, random combinations of these and perhaps other processes can give rise to apparent "regime shifts" in the PDO that are not predictable beyond about 2 years [Barlow et al., 2001; Schneider and Cornuelle, 2005; Newman, 2007; Alexander et al., 2008].

6. BEYOND THE PDO

The PDO is only one measure of variability in the North Pacific; other regions and/or modes of variability may result from North Pacific atmosphere-ocean dynamics. For example, Nakamura et al. [1997] first time-filtered the SST anomalies over the Pacific and then computed the first two EOFs for time scales >7 years. The first EOF shows strong variability along 40°–45°N in the west central Pacific along the subarctic front and little signal in the tropics, while the second EOF has a strong loading in the tropical Pacific and along the subtropical front in the central North Pacific. The first three rotated EOFs (where the patterns are no longer required to be orthogonal [e.g., see Richman, 1986; von Storch and Zwiers, 1999]) on unfiltered monthly SST anomalies over the Pacific basin are associated with ENSO, the PDO, and a North Pacific mode that exhibits pronounced decadal variability [Barlow et al., 2001]. The latter is similar to the leading pattern of variability identified by Nakamura et al. [1997], although its maximum amplitude is located farther east. In addition, variables such as salinity, thermocline depth, and SSH may provide a more direct estimate of dynamically driven ocean variability. Di Lorenzo et al. [2008] recently identified the North Pacific Gyre Oscillation (NPGO) as the dominant mode of SSH variability that has a dipole structure associated with out-of-phase changes in the strength of the subtropical and subpolar gyres in the eastern half of the basin. The NPGO also exhibits decadal variability. The mechanism(s) behind these extratropical decadal variations and the extent to which they are influenced by global warming requires further study.

Many of the processes that operate in the North Pacific are also found in the North Atlantic and the Southern oceans where they influence the large-scale SST anomaly

patterns. Heat flux forcing associated with fluctuations in the North Atlantic Oscillation (NAO) (with opposing SLP anomaly centers over the subtropics and Iceland) creates an SST tripole pattern with anomalies of one sign in midlatitudes, flanked by anomalies of the opposite sign in the subtropics and subpolar regions [e.g., *Cayan*, 1992b; *Seager et al.*, 2000]. Oceanic Rossby waves, gyre adjustments, and wind-driven currents also play an important role in decadal variability of the Gulf Stream [e.g., *Frankignoul et al.*, 1997; *Curry and McCartney*, 2001; *de Coëtlogon et al.*, 2006], although the direct connection between Rossby waves and the Gulf Stream is less apparent than in the KE region. The atmospheric bridge also influences the North Atlantic particularly in the subtropics, while there is also a NAO-like response in middle and high latitudes that is stronger during La Niña than during El Niño events [e.g., *Pozo-Vázquez et al.*, 2001; *Alexander et al.*, 2002; *Alexander and Scott*, 2008]. Modeling studies also indicate that the atmospheric response to tropical Atlantic SST anomalies influences air-sea interaction and SST variability in the North Atlantic [*Drevillon et al.*, 2003; *Peng et al.*, 2005, 2006]. In the Southern Hemisphere, the Southern Annular mode (with nearly zonally symmetric SLP anomalies with opposing centers between 30°S–50°S and 50°–90°S) and ENSO teleconnections drive SST anomalies in middle and high latitudes [*Ciasto and Thompson*, 2008]. In contrast to the Pacific, the meridional overturning circulation and interactions with sea ice have a much greater impact on low-frequency SST variability in the North Atlantic and parts of the Southern Ocean compared to the North Pacific.

REFERENCES

Alexander, M. A. (1990), Simulation of the response of the North Pacific Ocean to the anomalous atmospheric circulation associated with El Niþo, *Clim. Dyn.*, *5*, 53–65.

Alexander, M. A. (1992a), Midlatitude atmosphere-ocean interaction during El Niþo. Part I: The North Pacific Ocean, *J. Clim.*, *5*, 944–958.

Alexander, M. A. (1992b), Midlatitude atmosphere-ocean interaction during El Niþo. Part II: The Northern Hemisphere atmosphere, *J. Clim.*, *5*, 959–972.

Alexander, M. A., and C. Deser (1995), A mechanism for the recurrence of wintertime midlatitude SST anomalies, *J. Phys. Oceanogr.*, *25*, 122–137.

Alexander, M. A., and C. Penland (1996), Variability in a mixed layer model driven by stochastic atmospheric forcing, *J. Clim.*, *9*, 2424–2442.

Alexander, M. A., and J. D. Scott (1997), Surface flux variability over the North Pacific and North Atlantic oceans, *J. Clim.*, *10*, 2963–2978.

Alexander, M. A., and J. D. Scott (2008), The role of Ekman ocean heat transport in the Northern Hemisphere response to ENSO, *J. Clim.*, *21*, 5688–5707.

Alexander, M. A., C. Deser, and M. S. Timlin (1999), The re-emergence of SST anomalies in the North Pacific Ocean, *J. Clim.*, *12*, 2419–2433.

Alexander, M. A., J. D. Scott, and C. Deser (2000), Processes that influence sea surface temperature and ocean mixed layer depth variability in a coupled model, *J. Geophys. Res.*, *105*, 16,823–16,842.

Alexander, M. A., M. S. Timlin, and J. D. Scott (2001), Winter-to-winter recurrence of sea surface temperature, salinity and mixed layer depth anomalies, *Prog. Oceanogr.*, *49*, 41–61.

Alexander, M. A., I. Bladé, M. Newman, J. R. Lanzante, N.-C. Lau, and J. D. Scott (2002), The atmospheric bridge: The influence of ENSO teleconnections on air-sea interaction over the global oceans, *J. Clim.*, *15*, 2205–2231.

Alexander, M. A., N.-C. Lau, and J. D. Scott (2004), Broadening the atmospheric bridge paradigm: ENSO teleconnections to the North Pacific in summer and to the tropical west Pacific-Indian oceans over the seasonal cycle, in *Earth's Climate: The Ocean-Atmosphere Interaction*, edited by *Geophys. Monogr. Ser.*, vol. 147, edited by C. Wang, S.-P. Xie, and J. A. Carton, pp. 85–104, AGU, Washington, D. C..

Alexander, M. A., L. Matrosova, C. Penland, J. D. Scott, and P. Chang (2008), Forecasting Pacific SSTs: Linear inverse model predictions of the PDO, *J. Clim.*, *21*, 385–402.

Barlow, M., S. Nigam, and E. H. Berbery (2001), ENSO, Pacific decadal variability, and U.S. summertime precipitation, drought, and stream flow, *J. Clim.*, *14*, 2105–2128.

Barnett, T., D. W. Pierce, M. Latif, D. Dommonget, and R. Saravanan (1999), Interdecadal interactions between the tropics and the midlatitudes in the Pacific basin, *Geophys. Res. Lett.*, *26*, 615–618.

Barsugli, J. J., and D. S. Battisti (1998), The basic effects of atmosphere-ocean thermal coupling on midlatitude variability, *J. Atmos. Sci.*, *55*, 477–493.

Benson, A. J., and A. W. Trites (2002), Ecological effects of regime shifts in the Bering Sea and eastern North Pacific Ocean, *Fish Fish.*, *3*, 95–113.

Bhatt, U. S., M. A. Alexander, D. S. Battisti, D. D. Houghton, and L. M. Keller (1998), Atmosphere-ocean interaction in the North Atlantic: Near-surface climate variability, *J. Clim.*, *11*, 1615–1632.

Biondi, F., A. Gershunov, and D. R. Cayan (2001), North Pacific decadal climate variability since 1661, *J. Clim.*, *14*, 5–10.

Bjerknes, J. (1964), Atlantic air-sea interaction, *Adv. Geophys.*, *20*, 1–82.

Bladé, I. (1997), The influence of midlatitude coupling on the low-frequency variability of a GCM. Part I: No tropical SST forcing, *J. Clim.*, *10*, 2087–2106.

Bladé, I. (1999), The influence of midlatitude ocean-atmosphere coupling on the low-frequency variability of a GCM. Part II: Interannual variability induced by tropical SST forcing, *J. Clim.*, *12*, 21–45.

Capotondi, A., M. A. Alexander, and C. Deser (2003), Why are there Rossby wave maxima at 10°S and 13°N in the Pacific?, *J. Phys. Oceanogr.*, *33*, 1549–1563.

Capotondi, A., M. A. Alexander, C. Deser, and M. McPhaden (2005), Anatomy and decadal evolution of the Pacific subtropical cells, *J. Clim.*, *18*, 3739–3758.

Carton, J. A., and B. S. Giese (2008), A reanalysis of ocean climate using Simple Ocean Data Assimilation (SODA, *Mon. Weather Rev.*, *136*, 2999–3017.

Cayan, D. R. (1992a), Variability of latent and sensible heat fluxes estimated using bulk formulae, *Atmos. Ocean*, *30*, 1–42.

Cayan, D. R. (1992b), Latent and sensible heat flux anomalies over the northern oceans: The connection to monthly atmospheric circulation, *J. Clim.*, *5*, 354–369.

Cayan, D. R. (1992c), Latent and sensible heat flux anomalies over the northern oceans: Driving the sea surface temperature, *J. Phys. Oceanogr.*, *22*, 859–881.

Chelton, D. B., and R. E. Davis (1982), Monthly mean sea level variability along the west coast of North America, *J. Phys. Oceanogr.*, *15*, 2446–2461.

Chelton, D. B., and M. G. Schlax (1996), Global observations of oceanic Rossby waves, *Science*, *272*, 234–238.

Ciasto, L. M., and D. W. J. Thompson (2008), Observations of large-scale ocean-atmosphere interaction in the Southern Hemisphere, *J. Clim.*, *21*, 1244–1259.

Clarke, A. J., and S. van Gorder (1994), On ENSO coastal currents and sea levels, *J. Phys. Oceanogr.*, *24*, 661–680.

Curry, R. G., and M. McCartney (2001), Ocean gyre circulation changes associated with the North Atlantic Oscillation, *J. Phys. Oceanogr.*, *31*, 3374–3400.

Czaja, A. (2003), On the time variability of the net ocean to atmosphere heat flux in midlatitudes, with application to the North Atlantic basin, *Q. J. R. Meteorol. Soc.*, *129*, 2867–2878.

Dawe, J. T., and L. Thompson (2007), PDO-related heat and temperature budget changes in a model of the North Pacific, *J. Clim.*, *20*, 2092–2108.

de Coëtlogon, G., and C. Frankignoul (2003), On the persistence of winter sea surface temperature in the North Atlantic, *J. Clim.*, *16*, 1364–1377.

de Coëtlogon, G., C. Frankignoul, M. Bentsen, C. Delon, H. Haak, S. Massina, and A. Pardaens (2006), Gulf Stream variability in five oceanic general circulation models, *J. Phys. Oceanogr.*, *36*, 2119–2135.

Deser, C., and A. S. Phillips (2006), Simulation of the 1976/1977 climate transition over the North Pacific: Sensitivity to tropical forcing, *J. Clim.*, *19*, 6170–6180.

Deser, C., M. A. Alexander, and M. S. Timlin (1996), Upper-ocean thermal variations in the North Pacific during 1970–1991, *J. Clim.*, *9*, 1841–1855.

Deser, C., M. A. Alexander, and M. S. Timlin (1999), Evidence for wind-driven intensification of the Kuroshio Current Extension from the 1970s to the 1980s, *J. Clim.*, *12*, 1697–1706.

Deser, C., M. A. Alexander, and M. S. Timlin (2003), Understanding the persistence of sea surface temperature anomalies in midlatitudes, *J. Clim.*, *16*, 57–72.

Deser, C., A. S. Phillips, and J. W. Hurrell (2004), Pacific inter-decadal climate variability: Linkages between the tropics and the North Pacific during boreal winter since 1900, *J. Clim.*, *17*, 3109–3124.

Dickinson, R. E. (1978), Rossby waves–Long-period oscillations of oceans and atmospheres, *Annu. Rev. Fluid Mech.*, *10*, 159–195.

Di Lorenzo, E., et al. (2008), North Pacific Gyre Oscillation links ocean climate and ecosystem change, *Geophys. Res. Lett.*, *35*, L08607, doi:10.1029/2007GL032838.

Dommenget, D., and M. Latif (2002), Analysis of observed and simulated spectra in the midlatitudes, *Clim. Dyn.*, *19*, 277–288.

Drevillon, M., C. Cassou, and L. Terray (2003), Model study of the North Atlantic region atmospheric response to autumn tropical Atlantic sea-surface-temperature anomalies, *Q. J. R. Meteorol. Soc.*, *129*, 2591–2611.

Elsberry, R., and R. W. Garwood (1978), Sea surface temperature anomaly generation in relation to atmospheric storms, *Bull. Am. Meteorol. Soc.*, *59*, 786–789.

Enfield, D. B., and J. S. Allen (1980), On the structure and dynamics of monthly mean sea level anomalies along the Pacific coast of North and South America, *J. Phys. Oceanogr.*, *10*, 557–588.

Fine, R. A., J. L. Reid, and H. G. Östlund (1981), Circulation of tritium in the Pacific Ocean, *J. Phys. Oceanogr.*, *11*, 3–14.

Fine, R. A., W. H. Peterson, C. G. Rooth, and H. G. Östlund (1983), Cross-equatorial tracer transport in the upper waters of the Pacific Ocean, *J. Geophys. Res.*, *88*, 763–769.

Folland, C. K., J. A. Renwick, M. J. Salinger, and A. B. Mullan (2002), Relative influences of the Interdecadal Pacific Oscillation and ENSO on the South Pacific convergence zone, *Geophys. Res. Lett.*, *29*(13), 1643, doi:10.1029/2001GL014201.

Frankignoul, C. (1985), Sea surface temperature anomalies, planetary waves, and air-sea feedback in the middle latitudes, *Rev. Geophys.*, *23*, 357–390.

Frankignoul, C., and K. Hasselmann (1977), Stochastic climate models. Part 2. Application to sea-surface temperature variability and thermocline variability, *Tellus*, *29*, 284–305.

Frankignoul, C., and E. Kestenare (2002), The surface heat flux feedback. Part I: Estimates from observations in the Atlantic and the North Pacific, *Clim. Dyn.*, *19*, 633–647.

Frankignoul, C., and R. W. Reynolds (1983), Testing a dynamical model for mid-latitude sea surface temperature anomalies, *J. Phys. Oceanogr.*, *13*, 1131–1145.

Frankignoul, C., and N. Sennéchael (2007), Observed influence of North Pacific SST anomalies on the atmospheric circulation, *J. Clim.*, *20*, 592–606.

Frankignoul, C., P. Mller, and E. Zorita (1997), A simple model of the decadal response of the ocean to stochastic wind forcing, *J. Phys. Oceanogr.*, *27*, 1533–1546.

Fu, L.-L., and B. Qiu (2002), Low-frequency variability of the North Pacific Ocean: The roles of boundary- and wind-driven baroclinic Rossby waves, *J. Geophys. Res.*, *107*(C12), 3220, doi:10.1029/2001JC001131.

Garreaud, R. D., and D. S. Battisti (1999), Interannual (ENSO) and interdecadal (ENSO-like) variability in the Southern Hemisphere tropospheric circulation, *J. Clim.*, *12*, 2113–2123.

Gedalof, Z., N. J. Mantua, and D. L. Peterson (2002), A multi-century perspective of variability in the Pacific Decadal Oscillation: New insights from tree rings and coral, *Geophys. Res. Lett.*, *29*(24), 2204, doi:10.1029/2002GL015824.

Gill, A. E. (1982), *in Atmosphere-Ocean Dynamics*, 662 pp., Academic, New York.

Graham, N. E., et al. (1994), On the roles of tropical and mid-latitude SSTs in forcing interannual to interdecadal variability in the winter Northern Hemisphere circulation, *J. Clim.*, *7*, 1416–1441.

Gu, D., and S. G. H. Philander (1997), Interdecadal climate fluctuations that depend on exchanges between the tropics and extratropics, *Science*, *275*, 805–807.

Hanawa, K., and S. Sugimoto (2004), 'Reemergence' areas of winter sea surface temperature anomalies in the world's oceans, *Geophys. Res. Lett.*, *31*, L10303, doi:10.1029/2004GL019904.

Hasselmann, K. (1976), Stochastic climate models, *Tellus*, *28*, 473–485.

Huang, R. X., and B. Qiu (1994), Three-dimensional structure of the wind-driven circulation in the subtropical North Pacific, *J. Phys. Oceanogr.*, *24*, 1608–1622.

Iwasaka, N., and J. M. Wallace (1995), Large scale air sea interaction in the Northern Hemisphere from a view point of variations of surface heat flux by SVD analysis, *J. Meteorol. Soc. Jpn.*, *73*, 781–794.

Jacobs, G. A., H. E. Hurlburt, J. C. Kindle, E. J. Metzger, J. L. Mitchell, and A. J. Wallcraft (1994), Decade-scale trans-Pacific propagation and warming effects of an El Niþo anomaly, *Nature*, *370*, 360–363.

Ji, M., A. Leetmaa, and J. Derber (1995), An ocean analyses system for seasonal to interannual climate studies, *Mon. Weather Rev.*, *123*, 460–480.

Jin, F. F. (1997), A theory for interdecadal climate variability of the North Pacific ocean-atmosphere system, *J. Clim.*, *10*, 1821–1835.

Johnson, G. C., and M. J. McPhaden (2001), Interior pycnocline flow from the subtropical to the equatorial Pacific Ocean, *J. Phys. Oceanogr.*, *29*, 3073–3089.

Kalnay, E., et al. (1996), The NCEP/NCAR 40-year reanalysis project, *Bull. Am. Meteorol. Soc.*, *77*, 437–471.

Kelly, K. A. (2004), The relationship between oceanic heat transport and surface fluxes in the western North Pacific: 1970–2000, *J. Clim.*, *17*, 573–588.

Kistler, R., et al. (2001), The NCEP-NCAR 50-year reanalysis: Monthly means CD-ROM and documentation, *Bull. Am. Meteorol. Soc.*, *82*, 247–267.

Kleeman, R., J. P. McCreary, and B. A. Klinger (1999), A mechanism for the decadal variation of ENSO, *Geophys. Res. Lett.*, *26*, 1743–1747.

Klein, S. A., D. L. Hartmann, and J. R. Norris (1995), On the relationships among low-cloud structure, sea surface temperature and atmospheric circulation in the summertime northeast Pacific, *J. Clim.*, *8*, 1140–1155.

Klein, S. A., B. J. Soden, and N.-C. Lau (1999), Remote sea surface variations during ENSO: Evidence for a tropical atmospheric bridge, *J. Clim.*, *12*, 917–932.

Kushnir, Y., W. A. Robinson, I. Bladé, N. M. J. Hall, S. Peng, and R. Sutton (2002), Atmospheric response to extratropical SST anomalies: Synthesis and evaluation, *J. Clim.*, *15*, 2205–2231.

Kwon, Y. O., and C. Deser (2007), North Pacific decadal variability in the Community Climate System Model version 2, *J. Clim.*, *20*, 2416–2433.

Latif, M., and T. P. Barnett (1994), Causes of decadal climate variability over the North Pacific and North America, *Science*, *266*, 634–637.

Latif, M., and T. P. Barnett (1996), Decadal climate variability over the North Pacific and North America: Dynamics and predictability, *J. Clim.*, *9*, 2407–2423.

Lau, N. C., and M. J. Nath (1994), A modeling study of the relative roles of tropical and extratropical SST anomalies in the variability of the global atmosphere-ocean system, *J. Clim.*, *7*, 1184–1207.

Lau, N.-C., and M. J. Nath (1996), The role of the "atmospheric bridge" in linking tropical Pacific ENSO events to extratropical SST anomalies, *J. Clim.*, *9*, 2036–2057.

Lau, N.-C., and M. J. Nath (2001), Impact of ENSO on SST variability in the North Pacific and North Atlantic: Seasonal dependence and role of extratropical air-sea coupling, *J. Clim.*, *14*, 2846–2866.

Lee, D. E., Z. Liu, and Y. Liu (2008), Beyond thermal interaction between ocean and atmosphere: On the extratropical climate variability due to the wind-induced SST, *J. Clim.*, *21*, 2001–2018.

Liu, Z. (1994), A simple model of the mass exchange between the subtropical and tropical ocean, *J. Phys. Oceanogr.*, *24*, 1153–1165.

Liu, Z., and M. A. Alexander (2007), Atmospheric Bridge, Oceanic Tunnel and Global Climatic Teleconnections, *Rev. Geophys.*, *45*, RG2005, doi:10.1029/2005RG000172.

Liu, Z., and L. Wu (2004), Atmospheric response to North Pacific SST: The role of ocean-atmosphere coupling, *J. Clim.*, *17*, 1859–1882.

Liu, Z., L. Wu, R. Gallimore, and R. Jacob (2002), Search for the origins of Pacific decadal climate variability, *Geophys. Res. Lett.*, *29*(10), 1404, doi:10.1029/2001GL013735.

Luo, J. J., and T. Yamagata (2001), Long-term El Niþo–Southern Oscillation (ENSO)-like variation with special emphasis on the South Pacific, *J. Geophys. Res.*, *106*, 22,211–22,227.

Mantua, N. J., S. R. Hare, Y. Zhang, J. M. Wallace, and R. Francis (1997), A Pacific interdecadal climate oscillation with impacts on salmon production, *Bull. Am. Meteorol. Soc.*, *78*, 1069–1079.

McCreary, J. P., and P. Lu (1994), Interaction between the subtropical and equatorial ocean circulations: The subtropical cell, *J. Phys. Oceanogr.*, *24*, 466–497.

McPhaden, M. J., and D. Zhang (2002), Slowdown of the meridional overturning circulation in the upper Pacific Ocean, *Nature*, *415*, 603–608.

Mestas-Nuþez, A. M., and D. B. Enfield (1999), Rotated global modes of non-ENSO sea surface temperature variability, *J. Clim.*, *12*, 2734–2746.

Meyers, S. D., M. Liu, J. J. O'Brien, M. A. Johnson, and J. L. Spiesberger (1996), Interdecadal variability in a numerical model of the northeast Pacific: 1970–89, *J. Phys. Oceanogr.*, *26*, 2635–2652.

Miller, A. J., and N. Schneider (2000), Interdecadal climate regime dynamics in the North Pacific Ocean: Theories, observations, and ecosystem impacts, *Prog. Oceanogr.*, *47*, 355–379.

Miller, A. J., D. R. Cayan, T. P. Barnett, N. E. Graham, and J. M. Oberhuber (1994), Interdecadal variability of the Pacific Ocean: Model response to observed heat flux and wind stress anomalies, *Clim. Dyn.*, *10*, 287–302.

Miller, A. J., W. B. White, and D. R. Cayan (1997), North Pacific thermocline variations on ENSO timescales, *J. Phys. Oceanogr.*, *27*, 2023–2039.

Monterey, G. I., and S. Levitus (1997), in *Seasonal Variability of Mixed Layer Depth for the World Ocean*, *NOAA Atlas NESDIS*, vol. 14, 96 pp., 87 figs., NOAA, Silver Spring, Md.

Nakamura, H., H. G. Lin, and T. Yamagata (1997), Decadal climate variability in the North Pacific in recent decades, *Bull. Am. Meteorol. Soc.*, *78*, 2215–2226.

Nakamura, H., T. Miyasaka, Y. Kosaka, K. Takaya, and M. Honda (2010), Northern Hemisphere extratropical tropospheric planetary waves and their low-frequency variability: Their vertical structure and interaction with transient eddies and surface thermal contrasts, in *Climate Dynamics: Why Does Climate Vary?*, *Geophys. Monogr. Ser.*, doi:10.1029/2008GM000789, this volume.

Namias, J. (1959), Recent seasonal interactions between North Pacific waters and the overlying atmospheric circulation, *J. Geophys. Res.*, *64*, 631–646.

Namias, J. (1963), Large-scale air-sea interactions over the North Pacific from summer (1962) through the subsequent winter, *J. Geophys. Res.*, *68*, 6171–6186.

Namias, J. (1965), Macroscopic association between mean monthly sea surface temperature and the overlying winds, *J. Geophys. Res.*, *70*, 2307–2318.

Namias, J. (1969), Seasonal interactions between the North Pacific Ocean and the atmosphere during the 1960's, *Mon. Weather Rev.*, *97*, 173–192.

Namias, J., and R. M. Born (1970), Temporal coherence in North Pacific sea-surface temperature patterns, *J. Geophys. Res.*, *75*, 5952–5955.

Namias, J., and R. M. Born (1974), Further studies of temporal coherence in North Pacific sea surface temperatures, *J. Geophys. Res.*, *79*, 797–798.

Neelin, J. D., D. S. Battisti, A. C. Hirst, F. F. Jin, Y. Wakata, T. Yamagata, and S. Zebiak (1998), ENSO theory, *J. Geophys. Res.*, *103*, 14,261–14,290.

Newman, M. (2007), Interannual to decadal predictability of tropical and North Pacific sea surface temperatures, *J. Clim.*, *20*, 2333–2356.

Newman, M., G. Compo, and M. A. Alexander (2003), ENSO-forced variability of the Pacific Decadal Oscillation, *J. Clim.*, *16*, 3853–3857.

Norris, J. R., and C. Leovy (1994), Interannual variability in stratiform cloudiness and sea surface temperature, *J. Clim.*, *7*, 1915–1925.

Norris, J. R., Y. Zhang, and J. M. Wallace (1998), Role of clouds in summertime atmosphere-ocean interactions over the North Pacific, *J. Clim.*, *11*, 2482–2490.

Ortiz, M. J., and A. Ruiz de Elvira (1985), A cyclo-stationary model of sea surface temperature in the Pacific Ocean, *Tellus, Ser. A*, *37*, 14–23.

Park, S., and C. B. Leovy (2004), Marine low-cloud anomalies associated with ENSO, *J. Clim.*, *17*, 3448–3469.

Park, S., C. Deser, and M. A. Alexander (2005), Estimation of the surface heat flux response to sea surface temperature anomalies over the global oceans, *J. Clim.*, *18*, 4582–4599.

Park, S., M. A. Alexander, and C. Deser (2006), The impact of cloud radiative feedback, remote ENSO forcing, and entrainment on the persistence of North Pacific sea surface temperature anomalies, *J. Clim.*, *19*, 6243–6261.

Peng, S., and J. S. Whitaker (1999), Mechanisms determining the atmospheric response to midlatitude SST anomalies, *J. Clim.*, *12*, 1393–1408.

Peng, S., W. A. Robinson, and M. P. Hoerling (1997), The modeled atmospheric response to midlatitude SST anomalies and its dependence on background circulation states, *J. Clim.*, *10*, 971–987.

Peng, S., W. A. Robinson, S. Li, and M. P. Hoerling (2005), Tropical Atlantic SST forcing of coupled North Atlantic seasonal responses, *J. Clim.*, *18*, 480–496.

Peng, S., W. A. Robinson, S. Li, and M. A. Alexander (2006), Effects of Ekman transport on the NAO response to a tropical Atlantic SST anomaly, *J. Clim.*, *19*, 4803–4818.

Pierce, D. W. (2001), Distinguishing coupled ocean-atmosphere interactions from background noise in the North Pacific, *Prog. Oceanogr.*, *49*, 331–352.

Pierce, D. W., T. P. Barnett, and M. Latif (2000), Connections between the Pacific Ocean tropics and midlatitudes on decadal timescales, *J. Clim.*, *13*, 1173–1194.

Power, S. B., T. Casey, C. Folland, A. Colman, and V. Mehta (1999), Interdecadal modulation of the impact of ENSO on Australia, *Clim. Dyn.*, *15*, 319–324.

Pozo-Vázquez, D., M. J. Esteban-Parra, F. S. Rodrigo, and Y. Castro-Díez (2001), The association between ENSO and winter atmospheric circulation and temperature in the North Atlantic region, *J. Clim.*, *14*, 3408–3420.

Qiu, B. (2000), Interannual variability of the Kuroshio Extension system and its impact on the wintertime SST field, *J. Phys. Oceanogr.*, *30*, 1486–1502.

Qiu, B. (2003), Kuroshio Extension variability and forcing of the Pacific decadal oscillations: Responses and potential feedback, *J. Phys. Oceanogr.*, *33*, 2465–2482.

Qiu, B., and S. Chen (2005), Variability of the Kuroshio Extension jet, recirculation gyre and mesoscale eddies on decadal time-scales, *J. Phys. Oceanogr.*, *35*, 2090–2103.

Qiu, B., N. Schneider, and S. Chen (2007), Coupled decadal variability in the North Pacific: An observationally-constrained idealized model, *J. Clim.*, *20*, 3602–3620.

Qu, T., S.-P. Xie, H. Mitsudera, and A. Ishida (2002), Subduction of the North Pacific mode waters in a global high-resolution GCM, *J. Phys. Oceanogr.*, *32*, 746–763.

Rayner, N. A., P. Brohan, D. E. Parker, C. F. Folland, J. J. Kennedy, M. Vanicek, T. Ansell, and S. F. B. Tett (2006), Improved analyses of changes and uncertainties in sea surface temperature measured in situ since the mid-nineteenth century: The HadSST2 data set, *J. Clim.*, *19*, 446–469.

Reynolds, R. W. (1978), Sea surface temperature anomalies in the North Pacific Ocean, *Tellus*, *30*, 97–103.

Reynolds, R. W., T. M. Smith, C. Liu, D. B. Chelton, K. S. Casey, and M. G. Schlax (2007), Daily high-resolution-blend-ed analyses for sea surface temperature, *J. Clim.*, *20*, 5473–5496.

Richman, M. B. (1986), Rotation of principal components, *Int. J. Climatol.*, *6*, 293–335.

Robinson, I. S. (2004), *Measuring the Oceans From Space*, 669 pp., Springer, New York.

Saravanan, R. (1998), Atmospheric low frequency variability and its relationship to midlatitude SST variability: Studies using the NCAR Climate System Model, *J. Clim.*, *11*, 1386–1404.

Saravanan, R., and J. C. McWilliams (1997), Stochasticity and spatial resonance in interdecadal climate fluctuations, *J. Clim.*, *10*, 2299–2320.

Saravanan, R., and J. C. McWilliams (1998), Advective ocean-atmosphere interaction: An analytical stochastic model with implications for decadal variability, *J. Clim.*, *11*, 165–188.

Schneider, N., and B. D. Cornuelle (2005), The forcing of the Pacific Decadal Oscillation, *J. Clim.*, *18*, 4355–4373.

Schneider, N., and A. J. Miller (2001), Predicting North Pacific Ocean climate, *J. Clim.*, *14*, 3997–4002.

Schneider, N., A. J. Miller, M. A. Alexander, and C. Deser (1999), Subduction of decadal north Pacific temperature anomalies: Observations and dynamics, *J. Phys. Oceanogr.*, *29*, 1056–1070.

Schneider, N., A. J. Miller, and D. W. Pierce (2002), Anatomy of North Pacific decadal variability, *J. Clim.*, *15*, 586–605.

Seager, R., Y. Kushnir, M. Visbeck, N. Naik, J. Miller, G. Krahmann, and H. Cullen (2000), Causes of Atlantic Ocean climate variability between 1958 and 1998, *J. Clim.*, *13*, 2845–2862.

Seager, R., Y. Kushnir, N. H. Naik, M. A. Cane, and J. Miller (2001), Wind-driven shifts in the latitude of the Kuroshio–Oyashio Extension and generation of SST anomalies on decadal timescales, *J. Clim.*, *14*, 4249–4265.

Smith, T. M., et al. (1996), Reconstruction of historical sea surface temperatures using empirical orthogonal functions, *J. Clim.*, *9*, 1403–1420.

Solomon, A., J. P. McCreary, R. Kleeman, and B. A. Klinger (2003), Interactions between interannual tropical oscillations and decadal extratropical oscillations in an intermediate coupled model of the Pacific basin, *J. Clim.*, *16*, 2395–2410.

Solomon, A., S.-I. Shin, M. A. Alexander, and J. P. McCreary (2008), The relative importance of tropical variability forced from the North Pacific through ocean pathways, *Clim. Dyn.*, *31*, 315–331 doi:10.1007/s00382-007-0353-7.

Sugimoto, S., and K. Hanawa (2005), Remote reemergence areas of winter sea surface temperature anomalies in the North Pacific, *Geophys. Res. Lett.*, *32*, L01606, doi:10.1029/2004GL021410.

Sura, P., M. Newman, and M. A. Alexander (2006), Daily to decadal sea surface temperature variability driven by state-dependent stochastic heat fluxes, *J. Phys. Oceanogr.*, *36*, 1940–1958.

Taguchi, B., S.-P. Xie, H. Mitsudera, and A. Kubokawa (2005), Response of the Kuroshio Extension to Rossby waves associat-ed with the 1970s climate regime shift in a high-resolution ocean model, *J. Clim.*, *18*, 2979–2995.

Taguchi, B., S.-P. Xie, N. Schneider, M. Nonaka, H. Sasaki, and Y. Sasai (2007), Decadal variability of the Kuroshio Extension: Observations and an eddy-resolving model hindcast, *J. Clim.*, *20*, 2357–2377.

Tanimoto, Y., H. Nakamura, T. Kagimoto, and S. Yamane (2003), An active role of extratropical sea surface temperature anoma-lies in determining anomalous turbulent heat flux, *J. Geophys. Res.*, *108*(C10), 3304, doi:10.1029/2002JC001750.

Timlin, M. S., M. A. Alexander, and C. Deser (2002), On the reemergence of North Atlantic SST anomalies, *J. Clim.*, *15*, 2707–2712.

Trenberth, K. E. (1990), Recent observed interdecadal climate changes in the Northern Hemisphere, *Bull. Am. Meteorol. Soc.*, *71*, 988–993.

Trenberth, K. E., and J. W. Hurrell (1994), Decadal atmosphere-ocean variations in the Pacific, *Clim. Dyn.*, *9*, 303–319.

Trenberth, K. E., G. W. Branstator, D. Karoly, A. Kumar, N.-C. Lau, and C. Ropelewski (1998), Progress during TOGA in understanding and modeling global teleconnections associated with tropical sea surface temperatures, *J. Geophys. Res.*, *103*, 14,291–14,324.

Vimont, D. J., D. S. Battisti, and A. C. Hirst (2001), Footprinting: A seasonal link between the mid-latitudes and tropics, *Geophys. Res. Lett.*, *28*, 3923–3926.

Vimont, D. J., J. M. Wallace, and D. S. Battisti (2003), The seasonal footprinting mechanism in the Pacific: Implications for ENSO, *J. Clim.*, *16*, 2668–2675.

von Storch, H., and F. W. Zwiers (1999), *Statistical Analysis in Climate Research*, Cambridge Univ. Press, Cambridge, U. K.

Watanabe, M., and M. Kimoto (2000), On the persistence of decadal SST anomalies in the North Atlantic, *J. Clim.*, *13*, 3017–3028.

Weare, B. (1994), Interrelationships between cloud properties and SSTs on seasonal and interannual timescales, *J. Clim.*, *7*, 248–260.

Weng, W., and J. D. Neelin (1999), Analytical prototypes for ocean-atmosphere interaction at midlatitudes. Part II: Mechanisms for coupled gyre modes, *J. Clim.*, *12*, 2757–2774.

Wu, L., and Z. Liu (2003), Decadal variability in the North Pacific: The Eastern North Pacific mode, *J. Clim.*, *16*, 3111–3131.

Wu, L., Z. Liu, R. Gallimore, R. Jacob, D. Lee, and Y. Zhong (2003), Pacific decadal variability: The Tropical Pacific mode and the North Pacific mode, *J. Clim.*, *16*, 1101–1120.

Wu, L., D. Lee, and Z. Liu (2005), The 1976/77 North Pacific climate regime shift: The role of subtropical ocean adjustment and coupled ocean-atmosphere feedbacks, *J. Clim.*, *18*, 5125–5140.

Yulaeva, E., N. Schneider, D. W. Pierce, and T. Barnett (2001), Modeling of North Pacific climate variability forced by oceanic heat fluxes anomalies, *J. Clim.*, *14*, 4027–4046.

Zhang, Y., J. M. Wallace, and D. S. Battisti (1997), ENSO-like interdecadal variability, *J. Clim.*, *10*, 1004–1020.

M. Alexander, Earth System Research Laboratory, NOAA, R/PSD1, 325 Broadway, Boulder, CO 80305-3328, USA. (Michael.Alexander@noaa.gov)